

Article

Au and Te Minerals in Seafloor Massive Sulphides from Semyenov-2 Hydrothermal Field, Mid-Atlantic Ridge

Anna Firstova ^{1,2,*}, Tamara Stepanova ¹, Anna Sukhanova ¹, Georgy Cherkashov ^{1,2,*} and Irina Poroshina ¹

¹ Institute for Geology and Mineral Resources of the Ocean (FSBI “VNIIOkeangeologia”), 1 Angliiskiy Ave., 190121 St. Petersburg, Russia; steptv45@gmail.com (T.S.); sukhanova.anna.ru@gmail.com (A.S.); i.poroshina@gmail.com (I.P.)

² Institute of Earth Sciences, St. Petersburg State University, 7/9 Universitetskaya Emb., 199034 St. Petersburg, Russia

* Correspondence: anetfirst@gmail.com (A.F.); gcherkashov@gmail.com (G.C.); Tel.: +8-981-828-99-73 (A.F.); +7-812-713-8378 (G.C.)

Received: 4 March 2019; Accepted: 10 May 2019; Published: 15 May 2019



Abstract: The Semyenov-2 hydrothermal field located at 13°31′N of the Mid-Atlantic Ridge (MAR) is associated with an oceanic core complex (OCC) and hosted by peridotites and basalts with minor amounts of gabbro and plagiogranites. Seafloor massive sulphides (SMS) are represented by chimneys with zonality, massive sulphides without zonality and sulphide breccia cemented by opal and aragonite. The mean value of Au (20.6 ppm) and Te (40 ppm) is much higher than average for the MAR SMS deposits (3.2 ppm and 8.0 ppm, respectively). Generally, these high concentrations reflect the presence of a wide diversity of Au and Te minerals associated with major mineral paragenesis: primary native gold, melonite (NiTe₂) and tellurobismuthite (Bi₂Te₃) are related to high-temperature chalcopyrite (~350 °C); electrum (AuAg)₁, hessite (Ag₂Te) and altaite (PbTe) are related to medium- and low-temperature Zn-sulphide and opal assemblages (260–230 °C). Calaverite (AuTe₂) and Te-rich “fahlore” Cu₁₂(Sb,As,Te)₄S₁₃ are texturally related to the chalcopyrite-bornite-covellite. Enrichment of Au in sulphide breccia with opal and aragonite cement is driven by the re-deposition and the process of hydrothermal reworking of sulphide. The low-temperature fluid mobilizes gold from primary sulphide, along with Au and Te minerals. As a result, the secondary gold re-precipitate in cement of sulphide breccia. An additional contribution of Au enrichment is the presence of aragonite in the Cu-Zn breccia where the maximal Au content (188 ppm) is reached.

Keywords: seafloor massive sulphides; Mid-Atlantic Ridge; hydrothermal processes; gold; tellurides; aragonite; mechanism of precipitation; oceanic core complex

1. Introduction

Since the discovery of “black smokers” related to modern sea-floor hydrothermal activity within mid-oceanic ridges, their elevated contents of Au, Cu and Zn have been in spotlight. Numerous works investigated potential factors controlling high concentrations of Au in seafloor massive sulphides (SMS) [1–6]. At the MAR, high gold content is associated with different types of host rocks (Table 1)—ultramafic (within Logatchev, Ashadze-2 and Rainbow fields) and mafic (with Trans-Atlantic Geotraverse (TAG) field). A higher concentration of gold is commonly observed within ultramafic-hosted systems. Moreover, SMS at the MAR tend to demonstrate higher content of gold, compared to massive sulphide formations at the East-Pacific Rise (EPR).

Table 1. Gold and tellurium content of SMS (East-Pacific Rise, Mid-Atlantic Ridge).

Location	Au, ppm (<i>n</i>)	Te, ppm (<i>n</i>)	Reference
Mid-Ocean Ridges			
21°N, EPR	0.12 (46)	3.2 (46)	[6]
13°N, EPR	0.45 (71)	0.3 (71)	[6]
11°N, EPR	0.15 (18)	0.4 (18)	[6]
TAG, MAR	6.1	<0.1 (310)	[6,7]
Snakepit, MAR	1.66 (93)	4.2 (93)	[6]
Broken Spur, MAR	1.64 (76)	13.3 (76)	[6]
Rainbow * MAR	5.10	-	[8]
Krasnov, MAR	0.8 (162)	8.1 (8)	**
Logatchev-1 *, MAR	13 (53)	17 (17)	**
Logatchev-2 *, MAR	25.9	-	[9]
Ashadze-1 *, MAR	3.0 (120)	6.8 (53)	[10]**
Ashadze-2 *, MAR	10.0 (53)	7.6 (18)	**
Semyenov-2 *, MAR	21 (29)	40 (29)	This study

SMS, seafloor massive sulphides; EPR, East-Pacific Rise; MAR, Mid-Atlantic Ridge. * Ultramafic-hosted SMS at MAR; ** Massive sulphide database from VNIIOkeangeologia (Fe + Cu + Zn > 25%, *n* = 1051).

Gold in SMS of MAR deposits may associate with variable mineral assemblages: high-temperature Cu-Fe sulphide minerals at the Rainbow hydrothermal field, high-temperature Cu-rich sulphides and lower-temperature Zn-rich sulphides at Logatchev-1 field and with silica at Logatchev-2 field [5]. Elevated Au content is usually associated with high-temperature black smoker hydrothermal chimneys. Yet, some high Au contents (42 ppm) have been observed in white smoker chimneys at the TAG field as well [4]. It is generally known that gold deposition is controlled by metal enrichment in host rocks, favourable conditions for Au transport in the fluids, cooling/oxidation, mixing with seawater and the mechanism of precipitating [5,11]. Au usually occurs as native and electrum. Depending on mechanism of precipitating, Au could be also primary and secondary.

Au-enrichment in SMS from the Semyenov-2 hydrothermal field was noted in the work by Melekestseva et al. and Ivanov et al. [12,13]; however, only massive sulphides from station 287 were studied. Our study focuses on investigating the distribution of gold in chimneys with zonality, massive sulphides without zonality and sulphide breccia cemented by opal and aragonite. Here we, for the first time, study the gold distribution in samples of different mineral types from different stations across the Semyenov-2 hydrothermal field.

Another situation is relevant to Te distribution in SMS. Data regarding Te content and Te minerals in SMS are limited [8,14]. High tellurium contents in SMS, as well as in ancient volcanogenic massive sulphides (VMS), have been reported by Maslennikov [15]. In general, elevated Te contents were found in seafloor sulphides associated with both mafic (Broken Spur) and ultramafic rocks (Logatchev-1) (Table 1). The presence of coloradoite (HgTe) at the Rainbow hydrothermal field has been reported [2]. Rare Te minerals (including NiTe₂ and HgTe) in contact with native gold were observed in active Cu-rich black smoker chimneys at the Rainbow and Ashadze-1 fields as well [9,10].

The first data on Te content and Te minerals in the SMS of the Semyenov-2 hydrothermal field were noted by Firstova et al. [16]. Rare tellurides (tetradymite, hessite, stützite) have previously been found in the SMS of the Semyenov-2 hydrothermal field but have not been studied in detail [12,16]. In this study, we present the first data of Te mineral distribution in different mineral types within the Semyenov-2 hydrothermal field aiming to reveal factors controlling the distribution of Te minerals in high- and low- temperature sulphides.

2. Geological Background

The Semyenov hydrothermal area is located on the western flank of the MAR axial rift space, between the Fifteen-Twenty and Marathon Fracture zones at latitude 13°30'N (Figure 1A). The Semyenov

cluster consists of five hydrothermal fields. These fields are located along a smoothed crest of an east-west elongated dome-shaped corrugated mountain. This dome, a rugged massif adjacent to it from the west and the corrugated terrace-like lower surface to the north, were previously identified as an oceanic core complex [17–21]. The formation of such structures is generally attributed to long-term slips along large-scale detachment faults [22–25]. The corrugated dome is mainly composed of peridotites, with a small amount of gabbro. Its summit surface is partially covered by a relatively thin layer of basalts. Samples of very fresh lava and plagiogranites were recovered near its top [21,26]. Fresh basalts were also dredged on the sub meridional volcanic ridge to the south of the dome and in the basin to the south-west of it, which may indicate recent widespread flank volcanism in the area.

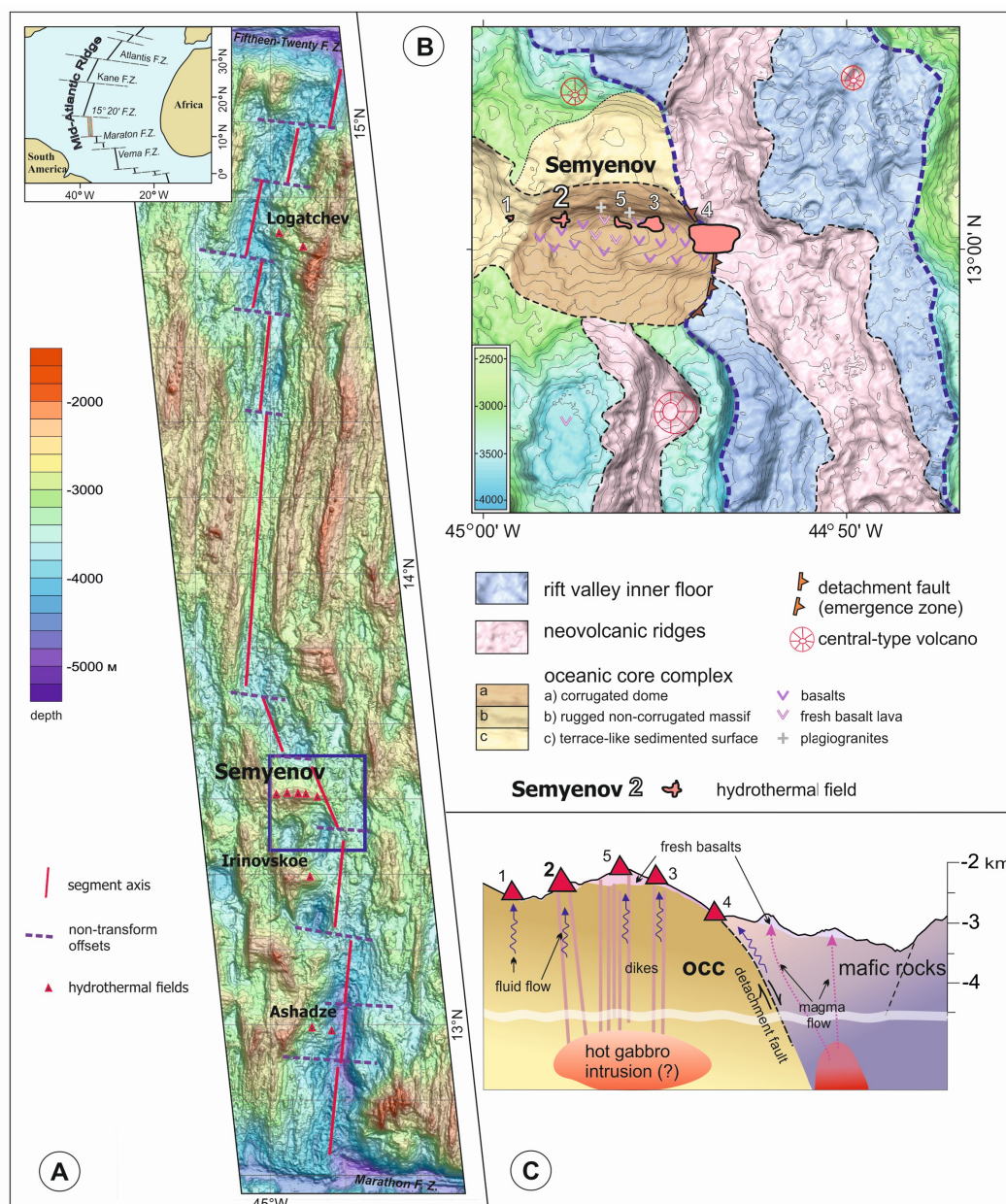


Figure 1. (A) Shaded-relief bathymetric map of the Mid-Atlantic Ridge between the Fifteen–Twenty Fracture Zone and the Marathon Fracture Zone, showing a second-order segmentation pattern and the location of the hydrothermal fields. The contour interval is 200 m. The box corresponds to the area of Figure 1B. (B) Morphostructural setting of the Semyenov hydrothermal fields. (C) Interpretative cross-section of the MAR rift valley in the Semyenov cluster (this figure was modified from Pertsev et al., 2012 [26]); vertical exaggeration 3:1.

The Semyenov-2 hydrothermal field lies near the western flank of the dome at 2300–2500 m water depth, some 8 km away from the spreading axis (Figure 1B). Both basalts and serpentinites were found in this area.

All the hydrothermal fields of the Semenov cluster are evidently controlled by a single latitudinal tectonically weakened zone. Hydrothermal activity in the Semyenov-2 hydrothermal field (as well as in the Semyenov-1, 3 and 5 fields) is presumably associated with the existence of a hot gabbro body directly under the dome (Figure 1C) [19].

The Semyenov-2 hydrothermal field contains two massive sulphide bodies, of 600 × 400 m and 200 × 175 m, respectively. An active smoker was detected at the 275 station. (Figure 2) [27].

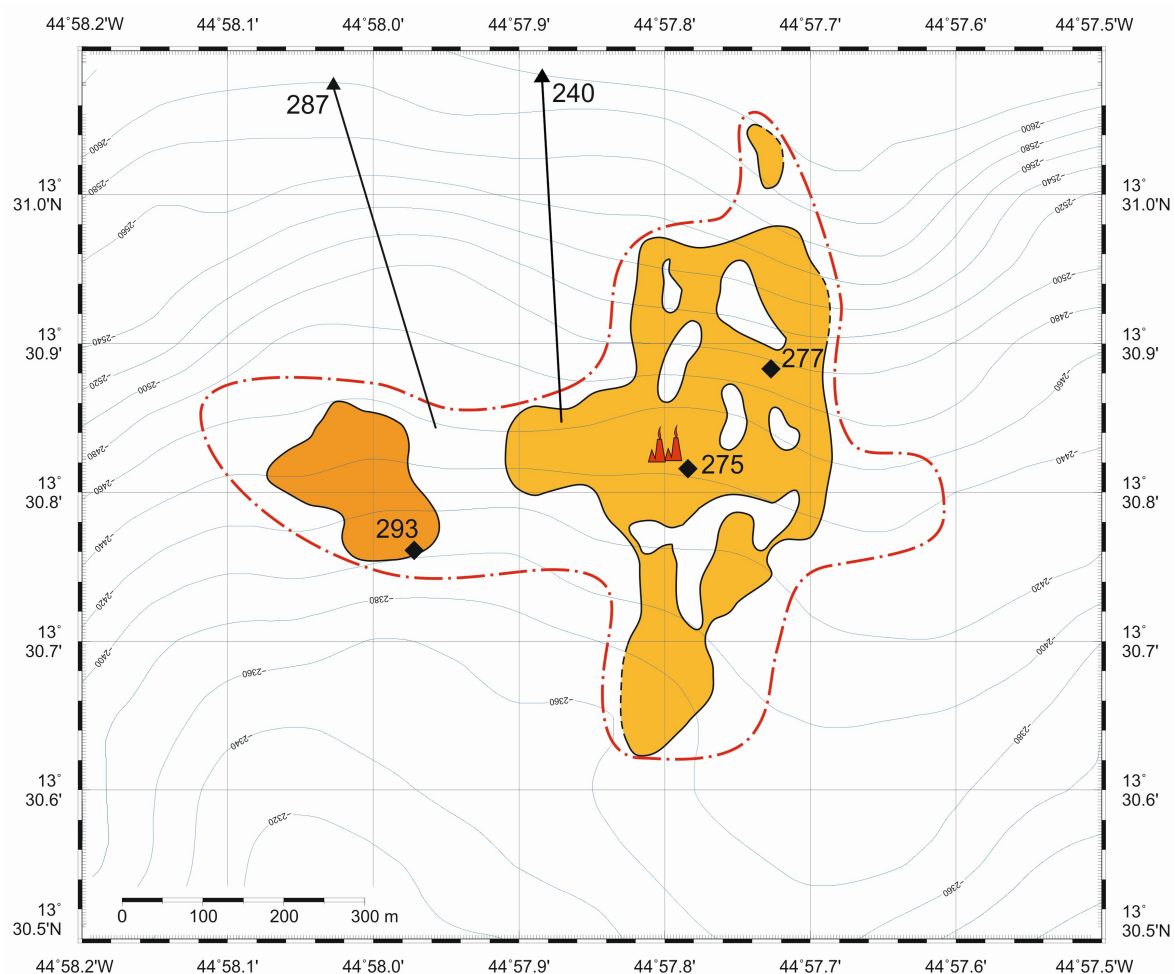


Figure 2. Semyenov-2 hydrothermal field. The red dashed line outlines the Semyenov-2 field. Red figures are active edifices detected by video profiling. Triangles with station numbers are the start point of dredging. Black lines show the tracks of dredging. Rhombs indicate grab samples with station numbers. This figure is simplified from unpublished Polar Marine Geosurvey Expedition (PMGE) open-file reports [28,29].

3. Materials and Methods

SMS samples were recovered by dredge (Station 287) and TV-grab (Stations 240, 277, 275, 293) during cruises 30 and 32 of RV Professor Logatchev [29,30]. In total, 29 sulphide samples were studied. An initial description of the mineralogy and structure of the samples was completed on board. The major and minor mineralogical phases were identified using reflected light microscopy. Whole rock chemistry (29 samples) was analysed at VNIIOkeangeologia, St. Petersburg, Russia. The SiO₂ was analysed using a standard photometric method using a Shimadzu uv-1650-pc spectrometer (Shimadzu, Kyoto, Japan). The samples were decomposed by melting with sodium carbonate. SiO₂ content was estimated using the

product of reduction of the yellow complex of silicon-molybdenum heteropoly-acid. Ascorbic acid was used as a reducing agent. We used gravimetric method to measure concentration of S by precipitating it with BaCl₂. Elements such as Fe, Cu, Zn, Pb, Cd, Ag, CaO and MgO were determined using atomic absorption spectroscopy (brand C-155 spectrometer with flame atomization). Quality control at the laboratory of VNIIOkeangeologia was performed by analysis of state standard (GSO) of water metal solutions (7254-96-Fe, 7255-96 Cu, 7256-96 Zn, 7252-96 Pb, 7472-98 Cd, 842-2002 Ag).

Tellurium was analysed on Agilent 7700 quadrupole inductively coupled plasma-mass spectrometer at VSEGEL, St. Petersburg, Russia. The test portion of a sample was 100 mg. The samples were digested in high density graphite or glass carbon autoclaves using 5 mL HNO₃ + 5 mL HClO₄ + 10 mL HF at 180 °C. All the pure acids used for digestion were additionally purified in BSB-939-IR apparatus (Berghof, Germany). The water for dilution was deionized in a DEMIWA 20-100 roa Watek Water Purification System (Watek, Ledec nad Sázavou, Czech Republic). The calibration of both instruments was completed with the reference solutions provided by the producers of the spectrometers. Quality control is based on the analysis of control samples of the International Geoanalytical Proficiency Testing Program and complies with the standard ISO 17025. For quality checking the method precision, a state certified sample of RUS-4 and a sample of SdAR-L2 (USA) from round 37A of the International Geoanalytical proficiency-testing program were used. The enlarged uncertainties (K = 2) of precision for all analyses did not exceed 30%. The whole rock Au content in 29 samples was determined by Atomic Absorption Spectroscopy (AAS) at the Central Laboratory of VSEGEL, using a Perkin Elmer Analyst-800 spectrometer. Quality control was performed by analysis of state standard (GSO) of flotation concentrate of Au-bearing ore CZK-3 (2739-83 Au).

Duplicate analyses were performed on 10% of the samples and the average error did not exceed ±1% for all techniques.

Major element analyses of ore-forming minerals were carried out on a Hitachi S3400N scanning electron microscope (SEM) equipped with an energy dispersive X-ray spectroscopy (EDX) detector AzTec Energy 350 and a wavelength dispersive X-ray spectroscopy (WDX) detector INCA 500 based at the Geomodel Centre, St. Petersburg State University, Russia. Vladimir Shylkovskiy and Natalia Vlasenko were the operators and used an acceleration potential of 20 kV, a beam current of 2 or 10 nA and a spot size from 3–5 µm for the EDX and WDX procedures, respectively. The following standards were used: Bi, Te, Au, Ag, Ni, Cu, InAs, Sb, Zn, Fe, FeS₂, Mo standards by Geller microanalytical laboratory and Bi, Se, FeS₂, CaSO₄ by MAC (Micro-Analysis Consultants Ltd.). The thin-section were carbon coated for SEM analysis and imaged using backscattered and secondary electrons (BSE).

The δ¹⁸O and δ¹³C were measured with a ThermoQuest Finnigan MAT DELTA (DELTA plus XL) mass spectrometer at the Centre of Isotopic Research of VSEGEL.

4. Results

4.1. SMS Samples: Structures, Textures and Mineralogy

The sulfide samples are represented by chimneys with zonality, massive sulphides without zonality and sulphide breccia. Studied samples were marked by characteristic mineralogy types. Chalcopyrite and chalcopyrite-sphalerite prevail in chimneys, isocubanite-chalcopyrite-sphalerite-wurtzite-opal dominate in massive sulfide, while the sulfide breccias cement (matrix) consist of amorphous silica (opal) and aragonite (Table 2).

The main feature of accessory mineralization is the occurrence of Au and Te minerals. Fahlore, sulphoarsenides and others also occur. Based on the results of the EDX and WDX analysis, minerals of rare elements were found in all sulphide samples (Table 3, Table S1). The size of these rare minerals is usually small (on average 5–10 µm).

Table 2. Cont.

SMS		Massive				Breccia							
Mineral Composition	Isocubanite-Chalcopyrite-Sphalerite-Wurtzite-Opal	Opal Cement				Aragonite Cement							
		Sphalerite-Wurtzite-Chalcopyrite-Isocubanite			Cu-sulphide			Isocubanite, Cu-sulphide			Cu-sulphide		
Station	287	287			287			240			293-KA		
Sample	M-1/1	M-1/1a	B-1	B-1/1	B-1/2	T-1, T-1a	T-1	T-2	M-1	M-1/1	KA-1,2		
Mineral													
Chalcopyrite, CuFeS ₂	++	++	+	+	+	+	+	+	+	+	+	+	
Isocubanite, CuFe ₂ S ₃	++	++	+++	+++	+++		+	+	+	+			
Sphalerite, (Zn,Fe)S	+++	+++	++	++	++		+	+	+	+			
Wurtzite, (Zn,Fe)S						+							
Pyrite, FeS ₂												+	
Marcasite, FeS ₂					+	++		+	+++			+	
Bornite, Cu ₅ FeS ₄	+			+	+				+	+			
Idaite, Cu ₃ FeS ₄				+	+								
Chalcocite, Cu ₂ S						++						++	
Djurleite, Cu ₃₁ S ₁₆												+	
Roxbyite, Cu ₉ S ₅													
Digenite, Cu ₉ S ₅								+	++			+	
Geerite, Cu ₈ S ₅												+	
Spionkopite, Cu _{1.4} S							+					+	
Yarrowite, Cu ₉ S ₈													
Covellite, CuS	+	+	++	+++	++		++	++	++	++	++	+	
Opal, SiO ₂ ·nH ₂ O	+++	+++	+++	++	++	+	++	+	++	+		+	
Aragonite, CaCO ₃						+++	+++	+++	+++	+++	+++	+++	
Barite, BaSO ₄	+								+				
Atakamite, Cu ₂ Cl(OH) ₃						+	+++	+++	+	+		+++	
Fe oxides and hydroxides							++	+	+	+	+	+	

Here (+++) indicates dominant mineral >25%; (++) indicates abundant mineral 25%–10%; and (+) indicates rare mineral <10%.

Table 3. Cont.

SMS		Massive			Breccia					
Mineral Composition	Station	Isocubanite-Chalcopyrite-Sphalerite-Wurtzite-Opal		Opal Cement	Cu-sulphide	Aragonite Cement				
		Sphalerite-Wurtzite-Chalcopyrite-Isocubanite		Cu-sulphide		Isocubanite, Cu-sulphide		Cu-sulphide		
Sample	287	287			287	240				293-KA
Mineral	M-1/1	M-1/1a	B-1, B-1/1, B-1/2		T-1, T-1a	T-1	T-2	M-1	M-1/1	KA-1,2
Native gold, Au	+	+	+	+	+	+	+	+		
Electrum, (AuAg) ₁	+	+	+	+				+	+	
Aurostibite, AuSb ₂				+						
Calaverite, AuTe ₂										
Sylvanite, AuAgTe ₄										
Hessite, Ag ₂ Te	+	+	+	+						
Melonite, NiTe ₂										
Tellurobismuthite, Bi ₂ Te ₃				+						
Tetradymite, Bi ₂ Te ₂ S				+						
Altaite, PbTe										
Clausthalite, PbSe		+		+						
Naumannite, Ag ₂ Se	+	+								
Se-galena	+	+		+						
Galena, PbS	+	+		+						
Fahlore, Cu ₁₂ (Sb,As) ₄ S ₁₃										
Glaucodote, (Co,Fe)AsS	+			+						
Cobaltite, CoAsS	+	+		+						

Note: +, the mineral presence.

4.1.1. Chimneys

Chalcopyrite chimneys. Most of the chimney samples were recovered on station 277 (Figure 3a) and are mainly represented by chimney fragments. The fragments range in size and reach 15 cm in diameter. Generally, somewhat vague zonal textures are observed. Yet, there is a distinct difference in the structure, texture and composition between small and large chimneys.

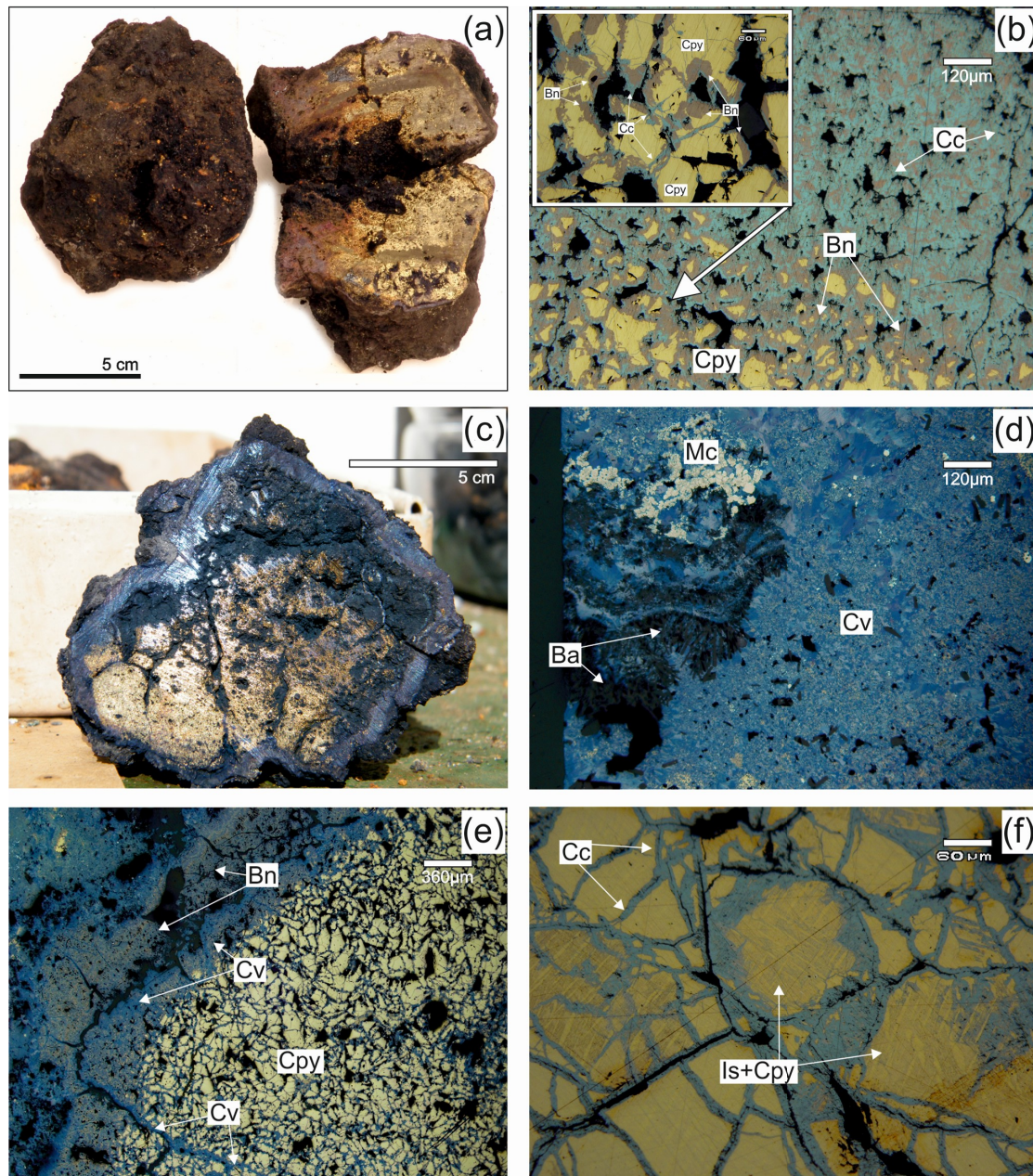


Figure 3. Chalcopyrite chimneys. (a) A general view of small chalcopyrite chimneys composed of chalcopyrite, bornite and Cu-sulphide; (b) Reflected light photograph. Chalcopyrite (Cpy) is partly replaced by bornite (Bn) and by minerals of the chalcocite (Cc) series (277-T-6); (c) A general view of large chalcopyrite chimney fragment composed of chalcopyrite in the central part and by low Cu-sulphide in the outer zone; (d) Reflected light photograph. The outer zone with Cu-sulphides of the covellite series, along with Barite (Ba) and marcasite (Mc) (277-T-3); (e) Reflected light photograph. Layered structure of a chimney with chalcopyrite (Cpy), covellite (Cv) and bornite (Bn) zones (277-T-3); (f) Reflected light photograph. Small chimney composed of isocubanite-chalcopyrite lattice aggregates, which are replaced by minerals of the chalcocite series (293-T-1).

Small chimneys consist of a central zone and a thin outer zone. In the central zone, massive, porous and fine to medium-grained chalcopyrite is dissected by channels and overgrown by subidiomorphic crystals. In some places, the chalcopyrite is replaced by a series of high Cu secondary sulphide minerals, such as chalcocite (Table 2, Figure 3b). The minor outer zone typically contains bornite, which is also replaced by chalcocite, djurleite and digenite (Figure 3b).

Large chimneys also demonstrate a similar two-zone structure (Figure 3c). The central zone is characterized by chalcopyrite and the outer zone is characterized by bornite. Scarce sphalerite with low Fe content (1–5 wt %) occurs around small channels in the central zone. However, unlike in the smaller chimneys, the samples are covered by a layer of low Cu-sulphide of the covellite series (up to 1 cm) (Table 2). Abundant covellite crystals (2–3 mm in diameter) are generally undergrown with tabular barite crystals (Figure 3d). Minerals of the covellite series develop into the inner part along the cracks, replacing chalcopyrite and bornite (Figure 3e). Locally, rare framboidal pyrite and marcasite are observed.

Chalcopyrite chimneys were also sampled at Station 293. However, along with chalcopyrite, these samples also contain substantial amounts of isocubanite. Chalcocite (CuS) develops along the primary minerals, in some instances replacing them (Figure 3f). Minerals of the covellite series were not found in these samples. Small pyrite crystals can be seen in the samples. Based on composition, these chimneys are similar to the small chimneys from Station 277.

Chalcopyrite chimneys are characterized by the occurrence of Au and Te minerals. Tellurobismuthite, calaverite, melonite and native gold were identified. The average compositions of accessory minerals are given in Table 4.

Table 4. Chemical composition of Au and Te minerals from the chalcopyrite chimneys.

Mineral (Number of Analyses)	Element (wt %)							Totals
	Bi	Te	Au	Ag	Ni	Cu	Fe	
Tellurobismuthite (10), Bi ₂ Te ₃	51.69	48.00	-	-	-	-	-	99.69
Calaverite (8), AuTe ₂	0.27	56.56	43.31	-	-	0.55	-	100.69
Native gold (8), Au	-	-	89.12	8.87	-	2.76	0.95	101.70
Melonite (2), NiTe ₂	-	81.40	-	-	18.41	-	-	99.81

Note: “-”, not detected.

Tellurobismuthite (Bi₂Te₃) is found in granular unaltered chalcopyrite from the central part (possibly the core) of the chimney (Figure 4a). Tellurides of Au—calaverite (AuTe₂) with an admixture of Cu and Bi (0.27 and 0.55 wt %, respectively)—were determined on the boundary of the chalcopyrite and digenite-jarleite (Figure 4a). In the central parts of chalcopyrite grains, melonite is identified (NiTe₂) (Figure 4b). Native gold was found in the pores of chalcopyrite aggregates, with an admixture of Cu (2.76 wt %) and Fe (0.95 wt %) (Figure 4c). In the outer zone, composed of low Cu-sulphides (predominantly covellite), there is a large amount of “fahlore” (Figure 4b). There is a positive correlation between the amount of covellite in the studied chimneys and the amount of “fahlore”. “Fahlore” located in the covellite zone always contains some amount of Te (Table S1). Sulfoarsenides, represented by glaucodote and cobaltite are found in the same outer zone.

Chimneys composed of isocubanite-chalcopyrite aggregates with high Cu-sulphide (chalcocite) are characterized by a stoichiometric composition of ore-forming minerals and an absence of the minerals of rare elements.

Sphalerite-chalcopyrite chimneys. Fragments of sphalerite-chalcopyrite chimneys were found on Station 277. The ratio between sphalerite and chalcopyrite varies. A zonal texture is observed. Sphalerite mainly overgrows chalcopyrite forming rhythmic-layered zones (Figure 5a). Cu-sulphides are mainly represented by covellite and are less abundant than in chalcopyrite chimneys. Active

chimneys discovered on Station 275 are characterized by “graphic” intergrowths of chalcopyrite and sphalerite (Figure 5b), while secondary Cu-sulphides are not observed.

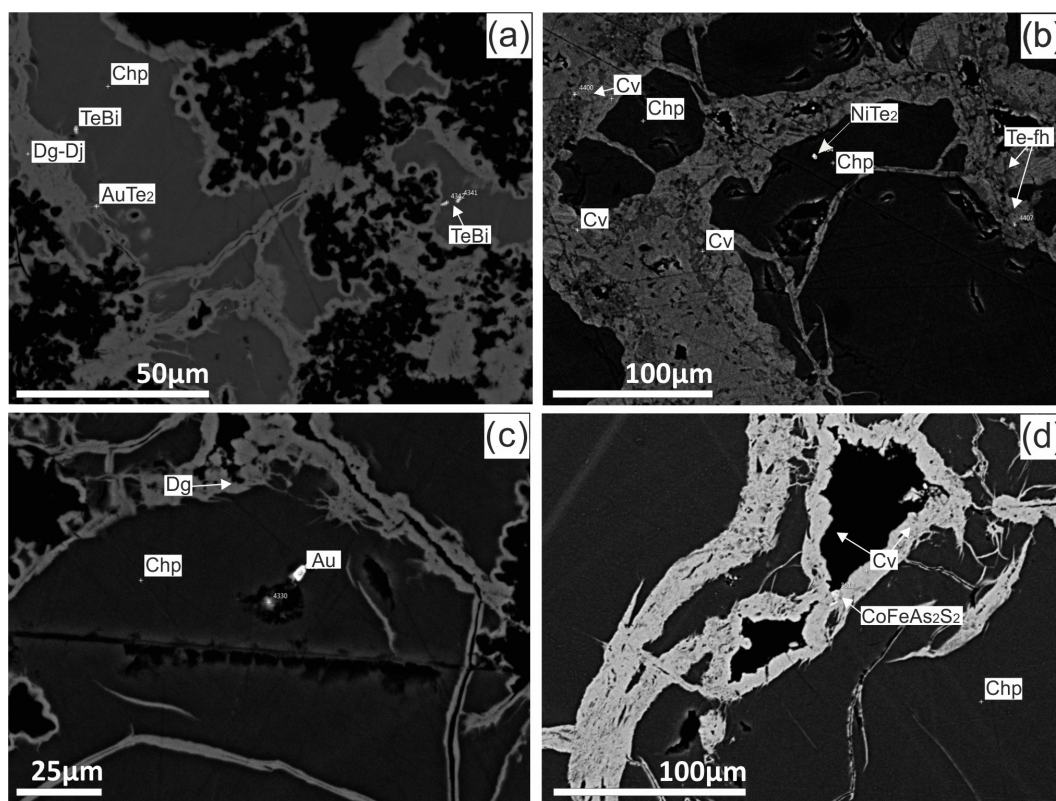


Figure 4. Au and Te minerals of chalcopyrite chimneys. BSE photographs. (a) Tellurobismuthite (Bi_2Te_3) in the centre of granular unaltered chalcopyrite (Chp) grains. Calaverite (AuTe_2) on the boundary of chalcopyrite replaced by digenite-jarleite (Dg-Dj); (b) Melonite (NiTe_2) in the chalcopyrite grain. Te-rich “fahlore” (Te-fh) located in the covellite zone; (c) Native gold (Au) in the pores of chalcopyrite aggregate; (d) Sulfoarsenides in the outer covellite zone.

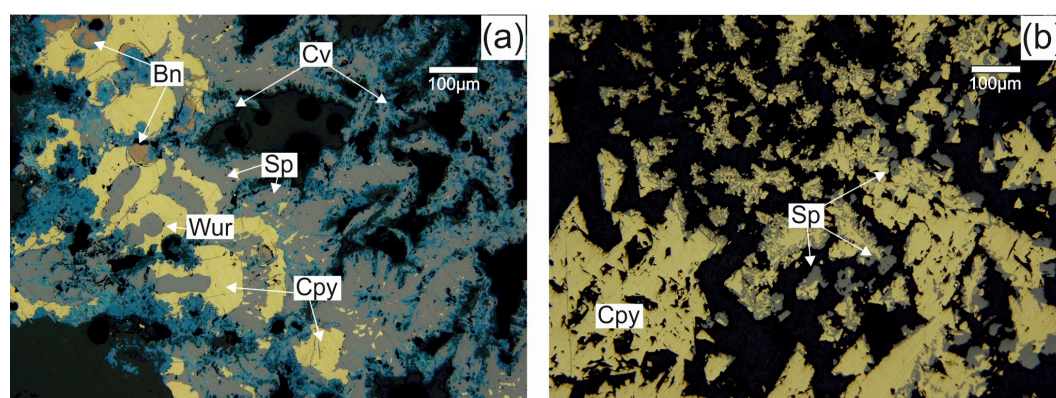


Figure 5. Reflected light photographs. (a) Rhythmic-layered texture of chalcopyrite (Cpy)-Zn-sulphides (sphalerite Sp, wurtzite Wur) aggregates. Wurtzite crystals are observed in the central part. Bornite (Bn) overgrows chalcopyrite (Cpy). Covellite (Cv) replaces sulphide minerals along fissures and overgrows Zn-sulphides (277-T-4); (b) “Graphic” intergrowths of sphalerite (Sp) and chalcopyrite (Cpy) in active chimneys (275-T-1).

In this type of chimney, Au and Te minerals (tellurobismutite, calaverite, hessite, altaite, native gold and electrum) were found. The average compositions of the minerals of rare elements are given in Table 5.

Table 5. Chemical composition of Au and Te minerals from the chalcopyrite-sphalerite chimneys.

Mineral (Number of Analyses)	Element (wt %)							Totals
	Au	Ag	Te	Bi	Pb	Se	S	
Native gold (6), Au	84.90	14.00	-	-	-	-	-	98.90
Electrum (8), (Au,Ag) ₁	65.95	33.82	-	-	-	-	-	99.77
Calaverite (6), AuTe ₂	45.03	-	54.69	-	-	-	-	99.72
Hessite (13), Ag ₂ Te	-	63.77	35.86	-	-	-	-	99.63
Tellurobismuthite (2), Bi ₂ Te ₃	-	-	45.46	54.54	-	-	-	100.00
Altaite (6), PbTe	-	-	38.11	-	61.46	-	-	99.57
Clausthalite (2), PbSe	-	-	-	-	72.12	27.60	-	99.72
Se-galena (9), Pb(S,Se)	-	-	-	-	84.76	3.92	11.14	99.82

Note: “-”, not detected.

In inactive chalcopyrite-sphalerite chimneys, native gold (rarely with Te and Bi) is associated with chalcopyrite (Figure 6a). Calaverite (AuTe₂) is abundant within bornite-chalcocite aggregates developed on chalcopyrite. Moreover, there is rare tellurobismuthite (Bi₂Te₃) in primary chalcopyrite grains (Figure 6b). Electrum is confined to the sphalerite-chalcopyrite intergrowths. Numerous examples of “fahlore” with tellurium content of up to 5.44 wt % are found in the covellite that develops along the cracks (Figure 6c, Table S1). Occasional grains of glaucodot, galena and Se-galena are also often detected.

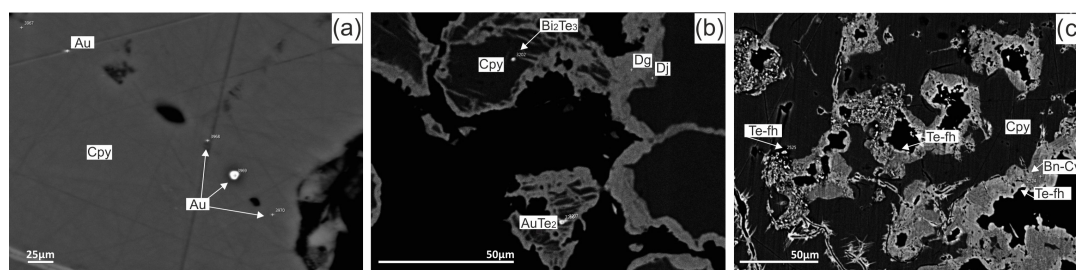


Figure 6. BSE photographs. Au and Te minerals of chalcopyrite-sphalerite chimneys (35.7 kyr). (a) Native gold (Au) associated with chalcopyrite (Cpy) grains; (b) Calaverite (AuTe₂) in the Cu-sulphide (digenite-jarosite). Rare tellurobismuthite (Bi₂Te₃) associated with chalcopyrite; (c) Abundant Te rich fahlore (Te-fh) in the covellite.

In active chimneys, hessite (Ag₂Te) and altaite (PbTe) are found. These minerals are located along the boundaries of chalcopyrite-sphalerite graphic intergrowths (Figure 7a). Noteworthy, intergrowths of electrum and clausthalite are found in the same locations. Galena, Se-galena and “fahlore” are also observed (Figure 7b). Tellurobismuthite (Bi₂Te₃) occasionally occurs within chalcopyrite grains.

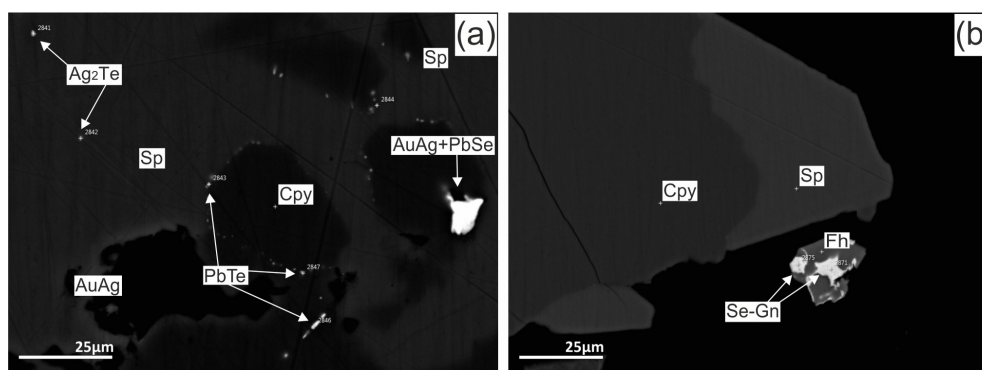


Figure 7. Au and Te minerals of chalcopyrite-sphalerite chimneys (active). BSE photographs. (a) Numerous hessite (Ag₂Te) and altaite (PbTe), intergrowths of electrum (AuAg) and clausthalite (PbSe) along the boundaries of chalcopyrite-sphalerite graphic intergrowths; (b) Se-galena (PbS,Se) and fahlore (fh) intergrowth.

4.1.2. Massive Sulphides

Isocubanite-chalcopyrite-sphalerite-wurtzite-opal massive sulphides are represented by samples up to 20 cm in size. These samples are comprised of porous fine-grained sulphides and coarse-grained sulphides in canals. Isocubanite constitutes a matrix in the exsolution texture. The matrix contains latticed intergrowths of lamella of chalcopyrite (Figure 8a). Granular Zn-sulphides are overgrown by Cu-Fe sulphides (Figure 8a). Based on observed crystal forms of Zn-sulphide, we identified it as sphalerite and wurtzite (Figure 8b). The wurtzite-sphalerite ratio is 6:1, based on the X-ray phase analysis by Melekestseva et al. [12]. Wurtzite crystals of up to 1 cm appear in the channels. These Zn-sulphides are characterized by a “spotty” distribution of Fe content (Figure 8c), reflected in the colour of the crystals and signs of mineral replacement. Fe content in zinc sulphides ranges from 7.5 to 20 wt %. Amorphous silica is represented by opal-A (X-ray analyses by Melekestseva et al. [30]) filling pores and channels (Figure 8a–d). Opal locally corrodes chalcopyrite and overgrows Zn-sulphides that are partially interlayered with opal aggregates (Figure 8a). Small wurtzite crystals (0.1–0.5 mm) and barite are often found in the opal matrix (Figure 8d). Secondary Cu-sulphides (covellite) tend to replace early sulphide minerals.

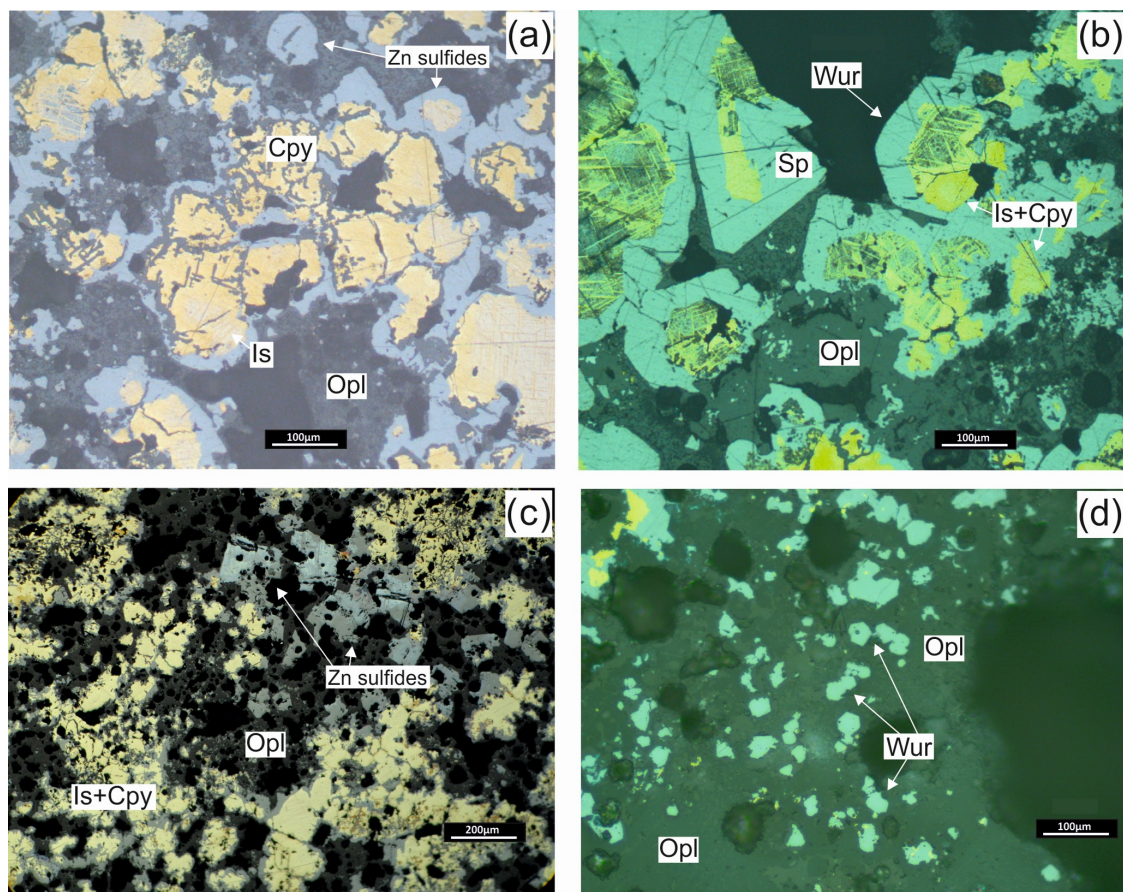


Figure 8. Isocubanite-chalcopyrite-sphalerite-wurtzite-opal massive sulphides. Reflected light photographs. (a) Subsequent formation of isocubanite-chalcopyrite (Is, Cpy) aggregates, Zn-sulphides and then opal (Opl) (287-M-1/2); (b) Idiomorphic forms of sphalerite (Sp) and wurtzite (Wur) around small canals (287-M-1/2); (c) Late generation of Zn-sulphide with a “patchy” feature of Fe-distribution in their composition. Zn-sulphide is associated with opal (Opl) infilled small canals and fissures (287-M-1/1); (d) Small wurtzite (Wur) crystals in the opal matrix (Opl) (287-M-1/1).

In massive sulphides, Au and Te occur in the form of native gold, electrum and hessite. The samples also contain naumannite and galena. The average compositions of the minerals of rare elements are given in Table 6.

Table 6. Chemical composition of Au and Te minerals from isocubanite-chalcopyrite-sphalerite-wurtzite-opal massive sulfide.

Mineral (Number of Analyses)	Element (wt %)						Totals
	Au	Ag	Te	Se	Mo	Bi	
Native gold (2), Au	89.38	10.58	-	-	0.08	0.03	100.07
Electrum (11), (Au,Ag) ₁	62.33	37.49	-	-	-	-	99.82
Hessite (9), Ag ₂ Te	-	62.79	37.11	-	-	-	99.90
Naumannite (24), Ag ₂ Se	-	72.06	-	27.66	-	-	99.72

Note: “-”, not detected.

In the isocubanite-sphalerite aggregates native gold is found, in some cases with an admixture of Mo and Bi (Figure 9a). The opal matrix contains abundant electrum and hessite (Figure 9b). Hessite also occurs in sphalerite grains. (Figure 9c). There are numerous selenides of silver (naumannite) in opal-sphalerite aggregates (Figure 9d).

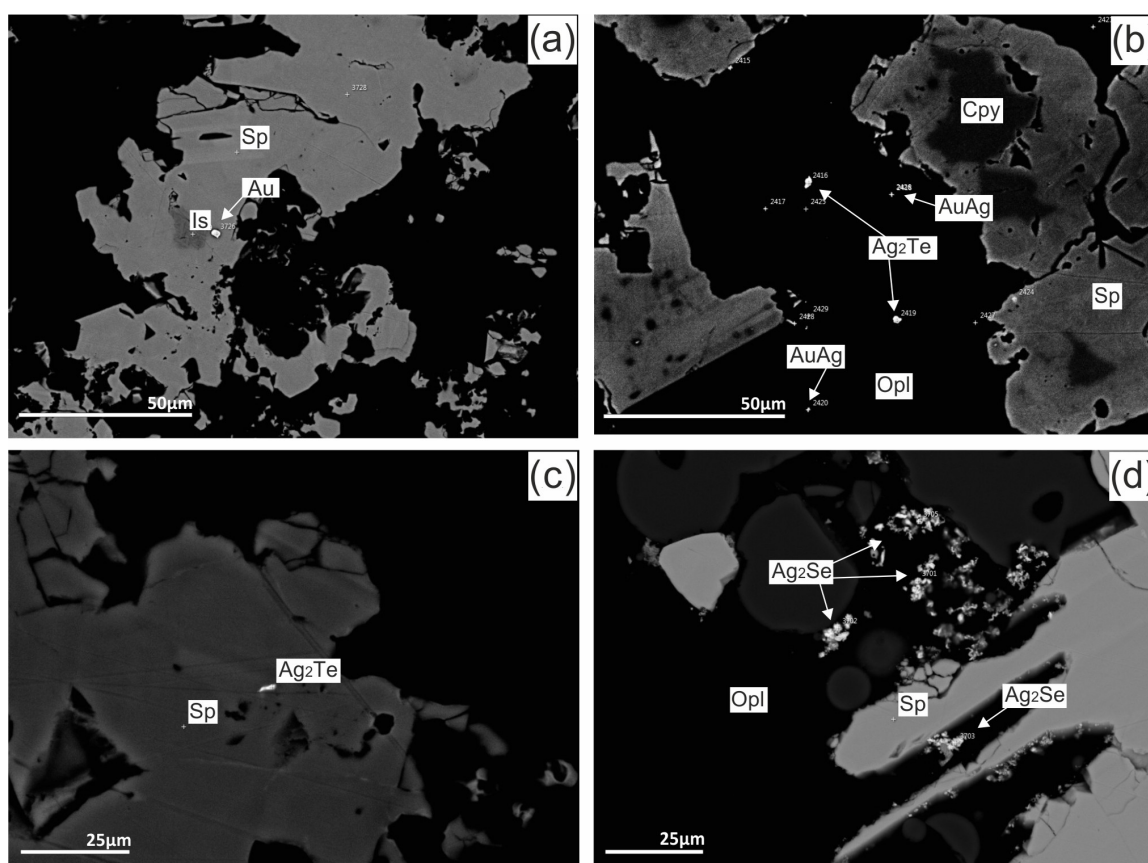


Figure 9. Au and Te minerals of isocubanite-chalcopyrite-sphalerite-wurtzite-opal massive sulphide. BSE photographs. (a) Native gold (Au) in the porous isocubanite-sphalerite aggregates; (b) Electrum (AuAg) and hessite (Ag₂Te) in opal cement; (c) Hessite associated with sphalerite; (d) Silver selenide (naumannite Ag₂Se) in opal-sphalerite aggregates.

4.1.3. Breccias

Sphalerite-wurtzite-chalcopyrite-isocubanite breccias with opal cement differ from the massive sulphides by their brecciated texture, ratio of sulphide minerals to opal. In this type, homogeneous isocubanite predominates (Figure 10a). Isocubanite is replaced along the cracks by covellite and bornite (Figure 10b). Sphalerite occurs in the altered clasts and is sometimes intergrown with chalcopyrite

(Figure 10c). The Fe content of zinc sulphides varies from 6 to 16 wt %. Pyrite and marcasite are rare in these samples. Large wurtzite crystals are found in pores in opal cement (Figure 10d).

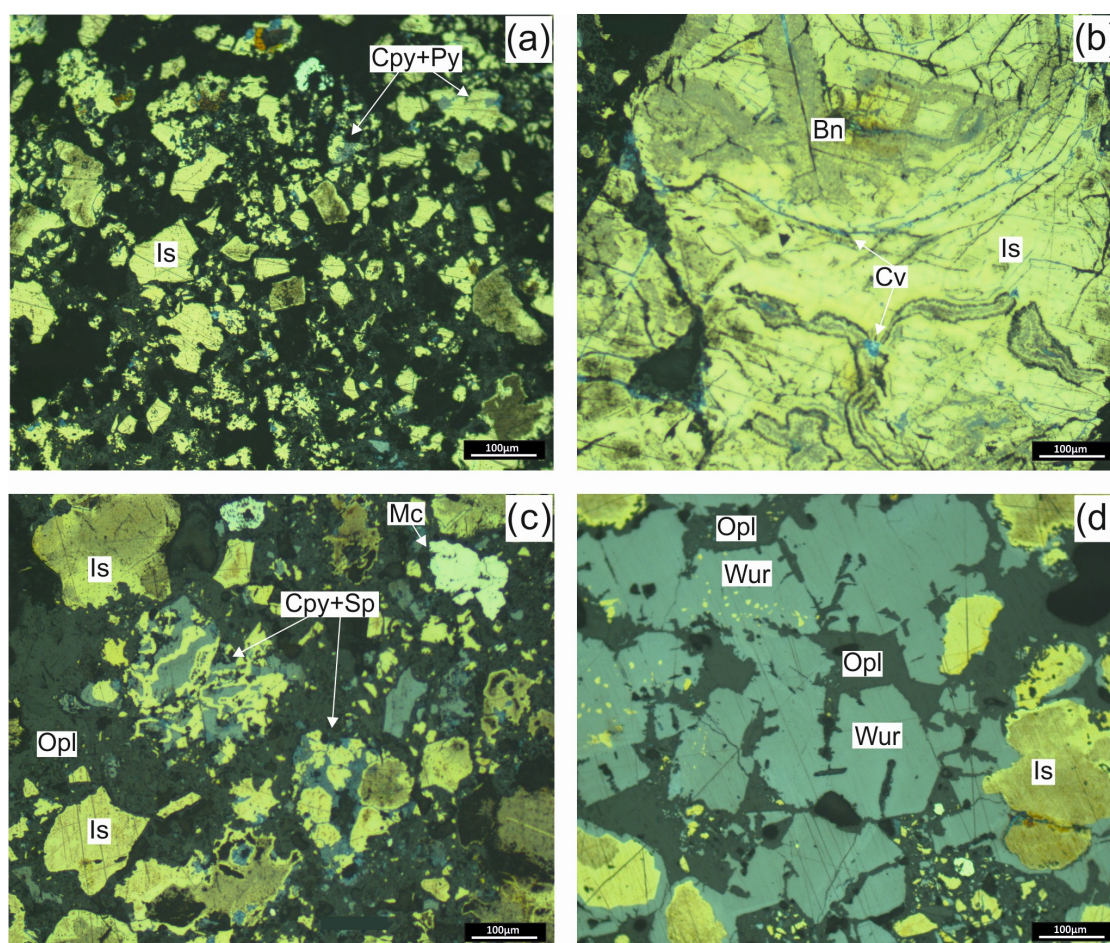


Figure 10. Sphalerite-wurtzite-chalcopyrite-isocubanite breccias with opal cement. Reflected light photographs. (a) Small clasts of altered isocubanite in opal cement (287-B-1/2); (b) Alteration of isocubanite (Is) along fissures, where its central parts are composed of covellite (Cv) (287-B-1/2); (c) Clasts of altered isocubanite (Is), along with chalcopyrite-sphalerite intergrowths (Cpy-Sp), Zn-sulphides and pyrite-marcasite clasts (287-B-2/1); (d) Wurtzite (Wur) crystals in opal cements around the channel (Opl) (287-B-2/1).

In contrast to massive sulphide of the same mineral type, sphalerite-wurtzite-chalcopyrite-isocubanite breccias with opal cement demonstrate less Te and Au minerals but contain native gold, aurostibite, hessite, tellurobismuthite and tetradytmite (Table 7).

Table 7. Chemical composition of Au and Te minerals from sphalerite-wurtzite-chalcopyrite-isocubanite breccias with opal cement.

Mineral (Number of Analyses)	Element (wt %)							Totals
	Bi	Te	Au	Ag	Sb	S	Mo	
Tellurobismuthite (3), Bi ₂ Te ₃	53.14	46.82	-	-	-	-	-	99.96
Tetradytmite (2), Bi ₂ Te ₂ S	60.52	34.78	-	-	-	4.57	-	99.87
Hessite (8), Ag ₂ Te	-	36.04	-	63.53	-	-	-	99.57
Native gold (3), Au	-	-	92.39	7.51	-	-	0.17	100.07
Aurostibite (1), AuSb ₂	-	-	47.36	0.18	52.26	-	-	99.80

Note: “-”, not detected.

Aurostibite was detected in isocubanite-sphalerite aggregates. A large amount of cobaltite and arsenopyrite, with admixture of Ni, Sb, Bi, was determined (Figure 11a). Rarely, native gold (sometimes with an admixture of Mo) appears in opal cement. Hessite is diagnosed at the boundary of sphalerite-isocubanite aggregates (Figure 11b). The rare grains of tellurobismuthite are associated with chalcopyrite from chalcopyrite-sphalerite intergrowths (Figure 11c). Tetradymite was found in isocubanite-chalcopyrite aggregates. In isocubanite-sphalerite aggregates, a large amount of cobaltite (Figure 11d) and arsenopyrite with impurities of Ni, Sb and Bi was determined.

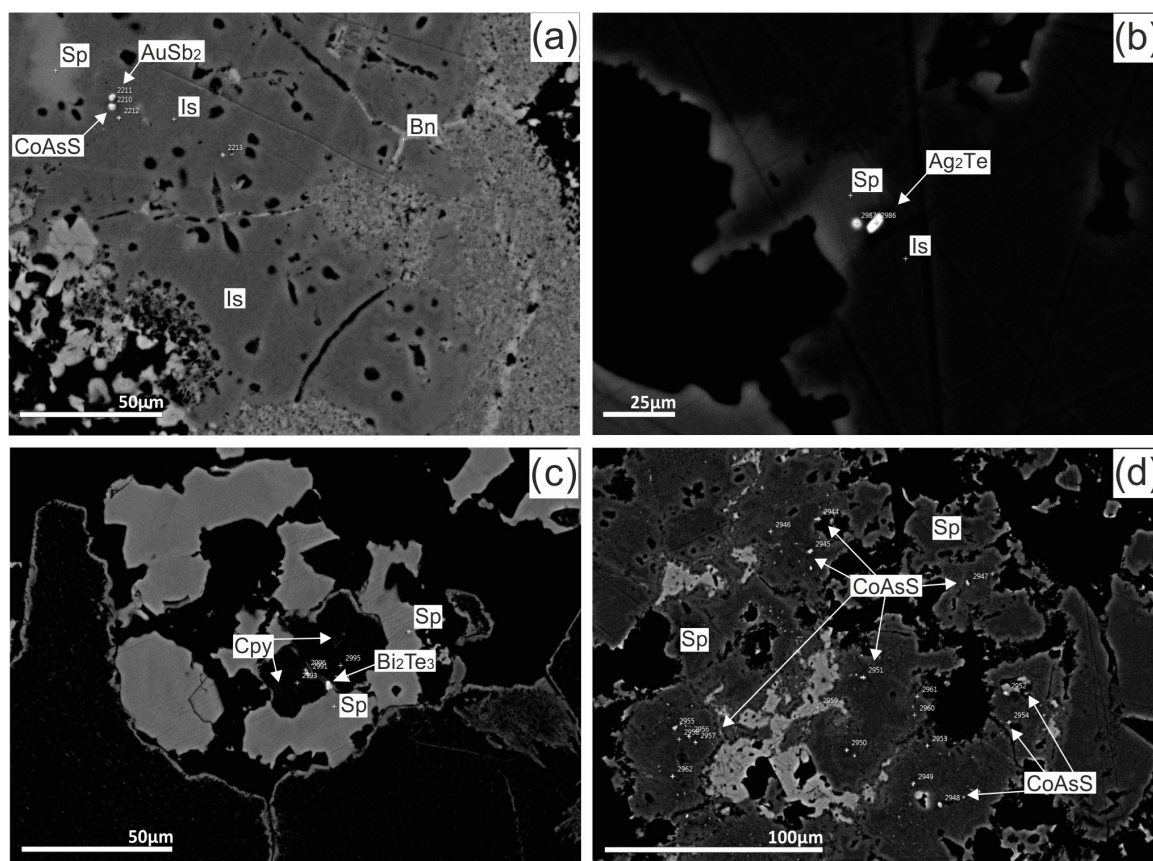


Figure 11. Au and Te minerals of sphalerite-wurtzite-chalcopyrite-isocubanite breccias with opal cement. BSE photographs. (a) Aurostibite (AuSb_2) and cobaltite (CoAsS) in the isocubanite-sphalerite aggregates; (b) Hessite (Ag_2Te) at the boundary of sphalerite-isocubanite aggregates; (c) Rare grains of tellurobismuthite (Bi_2Te_3) associated with the unaltered zone of chalcopyrite grains; (d) A large amount of cobaltite in the secondary Cu-sulphide.

Altered sulphide breccias with aragonite cement were sampled at three stations (Stations 240, 287, 293). All samples are composed of strongly altered fragments of Cu-rich chimneys or clasts of massive Cu-Zn sulphides in aragonite cement (Figure 12a–c). Yet, breccias from different stations demonstrate distinctly different sulphide mineral composition.

In the sample from Station 287, all fragments of massive chalcopyrite-sphalerite sulphides are replaced by secondary copper sulphides of the covellite series (Figure 12d). These fragments are sometimes overgrown by marcasite (Figure 12d). Minor fine-grained chalcopyrite and sphalerite is observed in some samples. The cement is composed of granular aragonite, radial crystals of aragonite and friable. The aragonite matrix contains impregnation of sulphides (Figure 12d). Opal, Fe-oxyhydroxides and atacamite are rarely observed.

In contrast to the breccia from station 287, breccia samples from Station 240 contain a significant amount of primary isocubanite relicts showing varying degree of replacement by Cu-sulphides or

Fe-oxyhydroxides (Figure 12e). Clasts of sphalerite are rare. Patchy Fe-oxyhydroxides and atacamite occur in the aragonite cement.

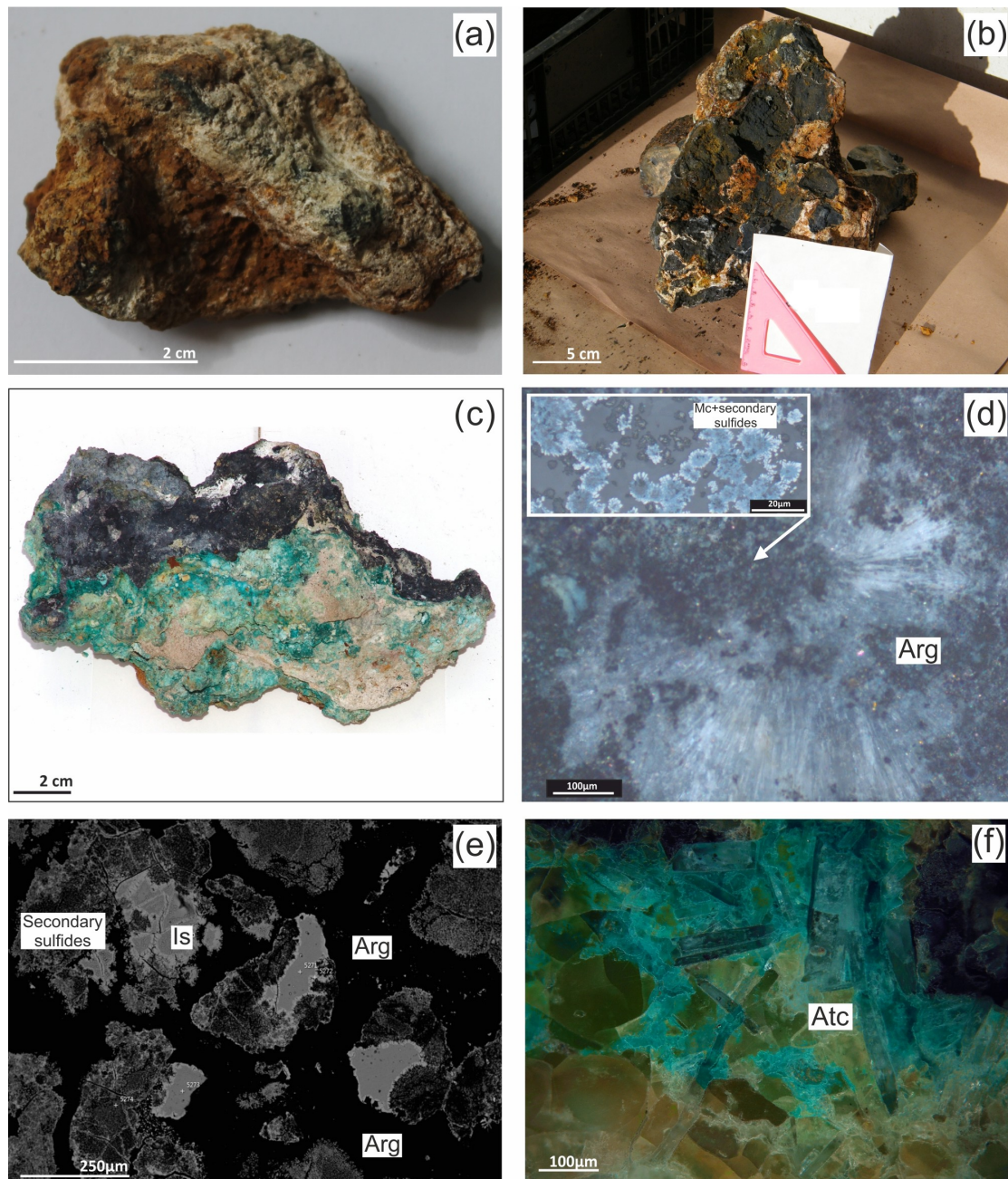


Figure 12. Altered sulphide breccia with aragonite cement. General view of samples (a) from 287 station; (b) from 240 station; (c) from 293 station; (d) Reflected light photographs; a fragment of massive chalcopyrite-sphalerite sulphide fully replaced by secondary copper sulphides in aragonite (Arg) in cement. Aragonite has radial crystals (287-T-1); (e) BSE photographs; clasts of isocubanite (Is) overgrown by Cu-sulphides of the covellite series in aragonite (Arg) (240); (f) Reflected light photographs; abundance of atacamite (Atc) in breccia from Station 293.

Breccia samples of Station 293 are characterized by abundant green atacamite (Figure 12f). Sulphide clasts are strongly altered and composed of secondary Cu-sulphides. Sometimes, a sulphide clast is overgrown by opal. Zn-sulphides are not observed.

Altered sulphide breccias with aragonite cement are characterized by the complete absence of tellurium minerals; however, a large amount of native gold was found. The average composition of native gold and electrum is listed in Table 8.

Table 8. Chemical composition of Au minerals of altered sulfide breccias with aragonite cement.

Mineral (Number of Analyses)	Element (wt %)		
	Au	Ag	Totals
Native gold (20), Au	94.19	5.35	99.54
Electrum (6), (Au,Ag) ₁	64.06	35.41	99.47

In the samples from Station 287-T, gold appears in the aragonite cement. More specifically, colloidal gold particles coat the aragonite crystals or fill the fractures developed within them (Figure 13).

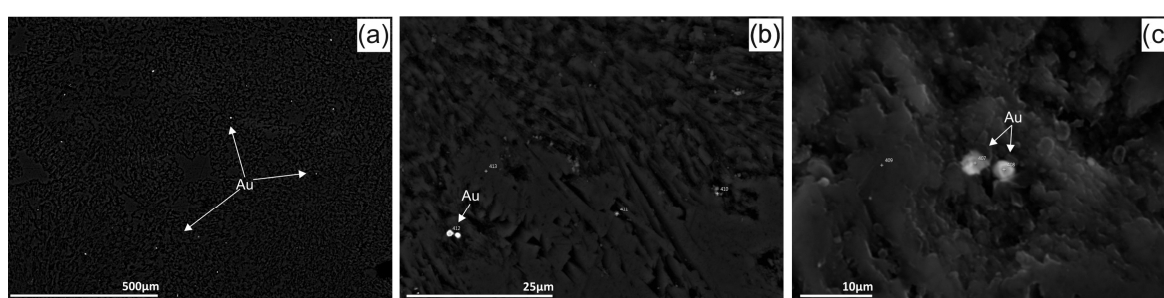


Figure 13. BSE photographs. (a–c) Abundant native gold in the interspace and on the surface of aragonite crystals.

Clausthalite and naumannite occurring in the secondary Cu-sulphides are relatively rare. Fissures of marcasite contain precipitates of native silver.

Samples from Station 240 contain native gold and electrum in aragonite cement (Figure 14). Silver as an impurity occurs in almost all secondary copper sulphides, completely replacing the primary chalcopyrite.

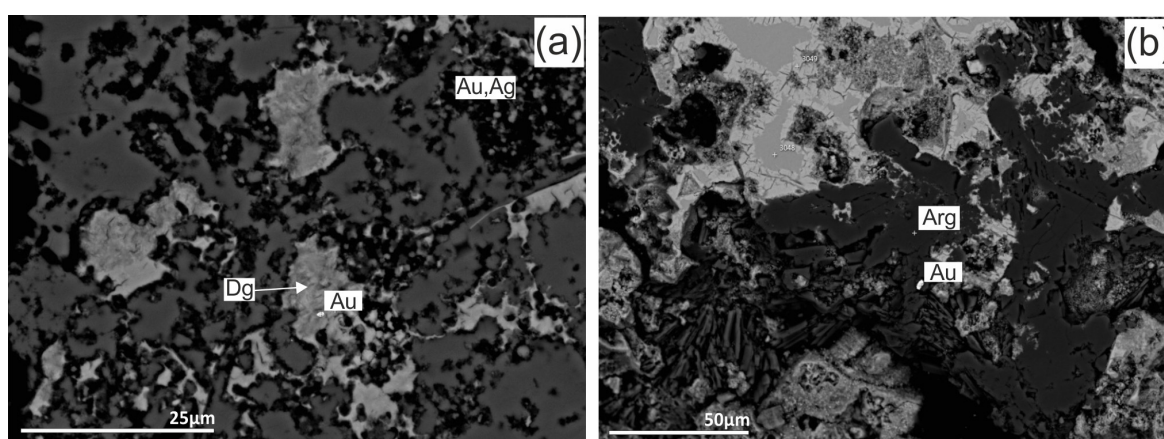


Figure 14. Au minerals of altered sulphide breccia with aragonite cement. BSE photographs. (a) Electrum (Au,Ag) in the secondary Cu-sulphide (digenite); (b) Native gold in aragonite cement.

However, samples from 293 station do not contain Au and any accessory minerals.

4.2. Composition and Isotopic Studies of Aragonite

Based on EDX analyses, aragonite from sulphide breccia contains Sr and Mg (Table 9). Sr content varies from 0.98 up to 2.02 wt % and Mg from 0.01 to 0.05 wt %. The $\delta^{18}\text{O}$ and $\delta^{13}\text{C}$ values were measured in aragonite from two samples (Table 9).

Table 9. Concentration of Ca, Mg, Sr and isotopic composition of aragonite with temperatures calculated based on this data.

Sample	Ca wt %	Mg wt %	Sr wt %	$\delta^{13}\text{C}$ ‰ (PDB)	$\delta^{18}\text{O}$ ‰ (PDB)	$\delta^{18}\text{O}$ ‰ (SMOW)	T (°C) Linear Equation
293-KA-1	36.92	0.01	1.83	+3.6	+3.7	+34.73	3.6
	41.05	0.05	1.25				
240-T	38.66	<LOD	1.25	n.d	n.d	n.d	n.d
	39.48	0.01	0.98				
240-M	41.80	<LOD	2.01				
	49.70	0.02	1.54				
287-T-1	36.72	0.04	1.84	+3.3	+3.4	+34.43	5.0
	39.65	<LOD	2.02				
	42.01	<LOD	1.27				
	45.09	<LOD	1.98				

Note: Limit of detection (LOD) = 0.01 wt %, n.d., not determined.

The temperature of aragonite deposition can be estimated from the oxygen isotope composition. Assuming that water has a $\delta^{18}\text{O} = 0\text{‰}$ (SMOW), temperatures were calculated from the $\text{CaCO}_3\text{-H}_2\text{O}$ relationship outlined by Böhm et al. [31].

Generally, aragonite cemented sulphide clasts show high concentration of Sr and low concentration of Mg, compared to aragonite precipitated in marine realm (e.g., aragonite of biogenic origin) (Figure 15a) [32]. Observed concentrations are close to those of aragonites associated with deep sea serpentinized ultramafic rock [32,33]. The $\delta^{18}\text{O}$ isotope signatures (Table 9) also correspond to aragonites associated with deep-sea serpentinized ultramafic rocks [32]. Relying on oxygen isotopic data from Bonnaty [32], we suggest that the aragonite was precipitated from seawater with a temperature of $\sim 5^\circ\text{C}$ (Table 9).

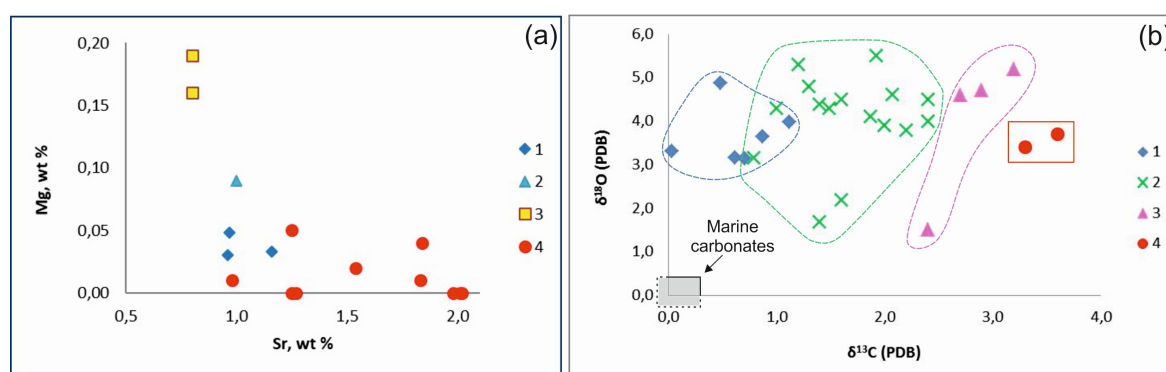


Figure 15. (a) Mg and Sr content of aragonite from sulphide breccia from Semyenov-2 hydrothermal field (4), compared with Mg and Sr concentration in aragonite from deep sea serpentinized ultramafic rock by Bonatti, 1980 (1) [32], and Thompson, 1970 (2) [33] and coral by Thompson, 1970 (3) [33]; (b) plot of $\delta^{18}\text{O}$ versus $\delta^{13}\text{C}$ values of (1) aragonite from deep sea serpentinized ultramafic rock [32], (2) carbonate chimneys of Lost City and Lost Village [35–37], (3) carbonate in-filling in fractured serpentine from Lost City [35], (4) aragonite from sulphide breccia of Semyenov-2 hydrothermal field (this study).

Both samples of aragonite from sulphide breccia demonstrate relatively heavy $\delta^{13}\text{C}$ composition: +3.3 and +3.6‰. Previous studies of $\delta^{13}\text{C}$ in aragonite from deep-sea ultramafic rock [32], specifically carbonate chimneys of the Lost City and Lost Village [34–36] and carbonate in-filling in fractured serpentine from the Lost City [36], report the $\delta^{13}\text{C}$ values ranging from +0.03 to +3.2‰. Comparing $\delta^{18}\text{O}$ versus $\delta^{13}\text{C}$ values of our samples with previously published results (Figure 15b), we find that the aragonites of Semyenov-2 hydrothermal field are relatively close to the samples of carbonates in-filling the fractures in serpentine at the Lost City. Früh-Green et al. [35] explained such high $\delta^{13}\text{C}$ values by CO_2 reduction to methane, which results in an enrichment of residual CO_2 in heavy carbon. This process typically accompanies serpentinization. However, the oxygen isotopic data does not support this explanation.

4.3. Sulfide Composition

4.3.1. Chimneys

Chalcopyrite chimneys of the Semyenov-2 hydrothermal field are characterized by a high content of Cu (avg. = 44.9–48.5 wt %), exceeding the bulk Cu content in SMS of the MAR (Table 10, Table S2). The maximum content of Au is slightly higher than the average content in SMS of the MAR (4.7 ppm). A diagnostic feature of these chimneys are the highest concentrations of Te (96 ppm), which is five times higher than average for SMS at the MAR (Table 10). More specifically, the samples of chimneys with covellite are characterized by higher concentrations of Te compared to the chalcopyrite chimneys with isocubanite and chalcocite.

Sphalerite-chalcopyrite chimneys are characterized by high concentrations of Zn. Samples from Station 277 have 1.01 wt % of Zn, whereas active smokers of 275 station show an even higher Zn content of 8.44 wt %. Cu concentrations are 36.9 wt % and 23.8 wt %, respectively. The average content of Au and Te is 10 ppm and 57 ppm, respectively. In an active chimney, the content of Au is 22.3 ppm and Te is 28 ppm. Active chimney is enriched in Zn-associated elements such as Pb (avg. = 240 ppm), Cd (avg. = 280 ppm) and Ag (avg. = 127 ppm) (Table 10, Table S2).

Table 10. Average bulk composition of SMS from Semyenov-2.

SMS		Chimneys			Massive			Breccia			SMS Semyenov-2	MAR *
Mineral Composition	Chalcopyrite	Chalcopyrite	Sphalerite-Chalcopyrite	Sphalerite-Chalcopyrite	Isocubanite-Chalcopyrite-Sphalerite-Wurtzite-Opal	Opal Cement	Aragonite Cement					
	Element	293	277	277	275 Active	287-M	287-B	Sphalerite-wurtzite-Chalcopyrite-Isocubanite	Cu-sulfide	Isocubanite, Cu-sulfide	Cu-sulfide	293, 277, 275, 287, 240
Fe, wt %	5.9	15.0	20.7	21.3	12.6	21.2	21.2	11.0	14.7	3.1	14.5	32.43
S	13.9	18.1	13.9	27.7	21.2	29.0	29.0	3.8	4.8	4.6	15.2	36.44
Cu	48.5	44.9	36.9	23.8	11.6	17.7	13.9	6.0	13.3	36.5	30.9	9.56
Zn	0.02	0.23	1.01	8.44	21.2	13.9	14.0	5.3	0.83	0.03	3.9	4.39
SiO ₂	16.7	3.7	1.4	12.6	29.4	17.0	14.0	17.0	5.5	15.9	9.5	6.8
CaO	0.17	0.08	0.03	0.08	0.09	<0.01	16.3	20.8	12.3	5.5	0.59	
MgO	0.22	0.09	0.12	0.18	0.09	0.05	2.5	0.53	1.5	0.42	0.23	
Pb, ppm	100	94	22	240	730	155	2400	36	155	312	157	
Cd	<2	7	23	280	670	545	120	7	<2	190	110	
Ag	26	50	16	127	371	294	1500	124	10	207	49	
Au	min/max average	0.8/2.9 1.8	0.7/4.7 2.9	5.8/14.4 10	- 22.3	15.6/32.9 24.3	17.1/60.5 39.2	128/188 158	0.4/188.2 8.6	0.9/1.7 1.3	0.4/188.2 20.8	0.1/66.0 * 3.2
Te	min/max average	15/29 22	12/96 61	56/59 57	- 28	20/22 21	25/28 26	23/24 24	22/25 24	14/16 15	12/96 40	9.4/250 * 8.0 **
N		2	10	3	1	2	3	2	4	2	29	1051 *

Note: *italic*, >10 times higher than average on Mid-Atlantic Ridge (MAR) sulfides; underlined, 5–10 times higher than average on MAR sulfides; **bold**, 1.5–5 times higher than average on MAR sulfides; n.d., no data; N, number of samples; * Massive sulfide database from VNIIOkeangeologia (Fe + Cu + Zn > 25%, n = 1051); ** Average for 178 samples of massive sulfide (Fe + Cu + Zn) > 25%.

4.3.2. Massive Sulphides

Massive isocubanite-chalcopyrite-sphalerite-wurtzite sulphides have high concentrations of Zn (avg. = 21.2 wt %) and the Cu content (avg. = 11.6 wt %). Along with the high abundance of Zn, the content of Si is almost four times higher than average for SMS of the MAR (Table 10). This reflects the presence of opal in samples. Thus, these sulphides are enriched in the elements with a strong correlation with Zn, such as Pb (avg. = 730 ppm), Cd (avg. = 670 ppm) and Ag (avg. = 371 ppm). The Au content (avg. = 24.3 ppm) is significant and the Te content is 21 ppm and less significant.

4.3.3. Breccia

In sphalerite-wurtzite-chalcopyrite-isocubanite breccias with opal cement, the average Zn concentration is 13.9 wt %, which is slightly less than Cu content (avg. = 17.7 wt %). As in massive sulphides, these samples have significant concentrations of Cd (avg. = 545 ppm), Ag (avg. = 294 ppm) and SiO₂ (avg. = 13.9 wt %). The maximum content of Au (60 ppm) is two times higher than in massive sulphides. The average content of Te is 26 ppm (Table 10, Table S2).

Breccias with aragonite cement from sample stations 293, 287 and 240 are rather different in terms of element composition. Breccia samples of 287 station are characterized by a close average content of Cu (6.0 wt %) and Zn (5.3 wt %). The occurrence of aragonite leads to high contents of CaO (avg. = 16.3 wt %). At the same time, a significant increase of the Pb, Ag and Mg concentrations is observed. These breccias have extremely high concentrations of Au (avg. = 158 ppm), which is more than 10 times higher than the average concentrations in SMS of the MAR (Table 10). This content is the highest for SMS within the MAR. The average concentration of Te is 24 ppm (Table S2).

Similar samples of breccia from 240 station contain low concentrations of Zn (avg. = 0.83 wt %) but significant Cu content (more than 13 wt %). In comparison with breccias from 287 station, these breccias have a lower concentration of Ag (avg. = 124 ppm). The average Au content is 8.6 ppm but in some samples, the values reach up to 20.6 ppm. The concentration of Te is 24 ppm.

Breccias from 293 station are characterized by high Cu content (avg. = 36.5 wt %) and the near absence of Zn (avg. = 0.03 wt %). The enrichment of CaO (avg. = 12.3 wt %) is notable (Table 10). These samples have the lowest Au content (avg. = 1.3 ppm) and Te (avg. = 15 ppm) content among the studied sulphide samples from Semyenov-2.

As compared to sulphides of the MAR, sulphides of the Semyenov-2 hydrothermal field are significantly enriched in Au and Te. The average content of Te is 40 ppm, which is five times higher than the average content of the MAR (8 ppm). The average concentration of Au is 20.8 ppm, which is eight times higher than the average value in SMS of the MAR (3.2 ppm) (Table 10).

Bulk geochemistry studies show that Au enrichments are primarily associated with Cu-Zn-Si assemblages, whereas the highest Te concentration occurs in Cu-rich samples. Moreover, the uniquely high concentrations of Au correlate with the appearance of Ca, along with the Cu-Zn-Si association in breccia.

4.3.4. Au Content in Host Rocks from the Semyenov-2 Hydrothermal Field

Basalt, serpentized peridotites, gabbro and plagiogranite were sampled within the hydrothermal field. Au content substantially varies among different types of rock. Yet, the average content of Au in the host rocks is close to Clarke value (Table 11). Comparing Au content of the host rocks from the seafloor within Semyenov-2 with their analogs from the other seafloor and onshore locations, we find that our study areas reveals slightly elevated Au concentrations.

Table 11. Gold content of Semyenov-2 host rocks in comparison with different data.

Rocks	Au, ppb	References
Abundance of element in the earth crust, Clarke	5	[38]
Mafic rocks	4	[39]
	4	[40]
MORB	1.2	[41]
Basalt	2.2	This study
Basalt	5.9	This study
Layered gabbroic complex	4.6	[41]
Gabbro	8	This study
Ultramafic rocks	5	[39]
	6	[40]
Peridotites from Logatchev hydrothermal field	4	[42]
Serpentinized peridotite	4.6	This study
Felsic rocks	4.5	[39]
	4.0	[40]
Plagiogranite	4.5	This study
Plagiogranite	6.8	This study

5. Discussion

5.1. The Condition of Formation SMS

Detailed mineralogical, geochemical studies and distribution of Au and Te minerals allow us to suggest variable conditions of formation SMS (the temperature of the fluid, mixing with seawater and the mechanism of precipitation) in chimneys with zonality, massive sulphides without zonality and sulphide breccia cemented by opal and aragonite.

The chimneys of the Semyenov-2 hydrothermal field are represented by variable mineral composition:

- chalcopyrite with isocubanite and predominantly chalcocite (high Cu-sulphide)
- chalcopyrite with mainly covellite (low Cu-sulphide)
- chalcopyrite-sphalerite.

Their mineral and geochemical features reflect the different temperatures of formation.

(a) The presence of isocubanite-chalcopyrite suggests the primarily high temperature of the fluid. At the same time, dominating chalcocite and the absence of low Cu-sulphide minerals (e.g., covellite) indicate a low oxidation potential resulting from insignificant mixing of the initial portion of fluid with seawater [37]. The Au content is 0.7–2.9 ppm. Au minerals are not observed. The Te content is 15–29 ppm. However, Te minerals and admixture of Te were not found. Based on the mineral and geochemical characteristics, we hypothesize that these chimneys formed by the short-term discharge of relatively reduced high-temperature (~350 °C) fluids [37,43]. Supposedly, minerals of Au and Te are not precipitated in high-temperature environment and reduced fluid state [43].

(b) These chalcopyrite chimneys are characterized by the presence of an outer zone composed of low Cu-sulphides of the covellite series. Some sphalerite, marcasite and barite are an indicator of the increasing oxidation potential and decreasing temperature of the fluid caused by its mixing with seawater. Abundant Te-rich fahlore and Co, Fe sulfarsenides (cobaltite and glaucodot) in the covellite zone are indicators of oxidative environments [15]. The Au content varies from 0.7 ppm up to 4.7 ppm. Rare native gold occurs in the unaltered chalcopyrite grains. The Te content is 12–96 ppm. These chimneys are characterized by the highest concentration of Te among all studied types and abundant tellurides: melonite, tellurobismuthite and calaverite. Previously, melonite was also detected in high-temperature chalcopyrite chimneys from the ultramafic-hosted Ashadze-1 and Rainbow hydrothermal fields [8,10]. Experimental data show that tellurides form at temperature intervals

below 350 °C [44] and above 230 °C [45]. Based on previous investigations, the favourable interval of temperature for tellurides precipitation is around 250 °C [15,44,45]. Melonite and tellurobismuthite are associated with the central part of the high-temperature chalcopyrite aggregates, where rare native gold also occurs. Calaverite occurs at the Cu-sulphide-chalcopyrite boundaries, reflecting the increasing oxidative conditions. We suggest that these chimneys formed from fluid with a temperature ~300–250 °C that experienced mixing with the seawater.

(c) The main feature is the presence of sphalerite as a major mineral, along with chalcopyrite. The texture allows us to suggest sequential precipitation chalcopyrite at temperature above 250 °C and subsequent formation of sphalerite at lower temperature. The outer zone, composed of covellite, bornite, barite and marcasite shows the mixing of hydrothermal fluid and seawater. This mineralogical paragenesis is a common characteristic of mixing hydrothermal fluid with seawater [46]. The Au content varies from 5.8 ppm to 14.4 ppm. The Te content is 55–59 ppm. The increasing gold content reflects the occurrence of electrum and calaverite. An active sphalerite-chalcopyrite chimney is characterized by the presence of other tellurides, such as hessite and altaite. These tellurides are associated with sphalerite. Cu-sulphide content is insignificant. The concentration of Au and Te in an active chimney is 22.3 ppm and 28 ppm, respectively. The enrichment of Zn-associated elements such as Pb, Cd and Ag point to the temperature of fluid being <250 °C. In addition, high Zn and Si could reflect sustained fluid flux [11,45]. Therefore, we suggest that the sphalerite-chalcopyrite chimneys and related tellurides formed at temperature around 250 °C with the following decreasing temperature of hydrothermal fluid.

Massive sulphide and sulphide breccia with opal cement are characterized by an isocubanite-chalcopyrite-sphalerite-wurtzite composition. Sulphide clasts and fragments of primary sulphide were altered. In massive sulphide, the Au content is ranging from 15.6 ppm to 32.9 ppm; the Te content is 20–22 ppm. Primary mineralization is characterized by Au and Te minerals similar to the ones observed in the sulphide chimney. Based on our investigation of chimneys and primary massive sulphide, we can conclude that the initial precipitation of Au and Te minerals is driven by the formation of primary native gold, melonite and tellurobismuthite related to chalcopyrite (~250–300 °C). During the fluid cooling (<250 °C), this environment occurs to be favourable for electrum, hessite and altaite precipitation related to sphalerite and partly to opal. The composition of an active chimney indicates that the precipitation happens from a conductively cooling fluid with an insignificant input of seawater. At the same time, penetration of seawater and mixing with fluid lead to increasing oxidative conditions and precipitation of calaverite and Te-rich fahlore together with covellite in the outer zones. Massive sulphides could form under variable temperature conditions: from high-temperature to low-temperature.

Breccia was formed as the result of destroying primary massive sulphide by the next portion of fluid, followed by cementing. In the sulphide breccia, the Au content is from 17.1 ppm to 60.5 ppm; the Te content is 25–28 ppm. Based on texture, mineralogical and geochemical composition of the sulphide breccia with opal cement, we conclude that these samples are products of hydrothermal reworking of sulphides [11]. The increasing Au content and fineness of Au minerals is associated with 'zone-refining' due to hydrothermal reworking of the primary Au-rich sulphide, followed by remobilization by a late low-temperature fluid and re-precipitating. This native gold could be considered as secondary. In addition, aurostibite in pores of chalcopyrite points towards a process of the primary gold replacement. Te occurs as an occasional tetradymite in re-deposited sulphide. Tellurides are not observed.

In addition to sulphide breccia with opal cement, samples of sulphide breccia with aragonite cement were also found. These samples are characterized by the highest Au content of 128–188 ppm. Elevated content of Te is also recorded and just like in breccia with opal cement, minerals and admixture of Te is not detected. In sulphide breccia with aragonite, sulphide clasts and fragments of sulphide are strongly altered and oxidized. The cement is represented by unaltered and coarse-grained aragonite. Based on oxygen isotopic data, we suggest that the aragonite formed from seawater with the temperature of ~5 °C, which circulated in fissures within the host rock during the hydrothermal activity of system. High values of $\delta^{13}\text{C}$ are remain lacking a solid interpretation. Here we speculate that the influence of the serpentinization

process within ultramafic host rock may play a part. Numerous colloidal of native gold are associated with the aragonite matrix and occur on the surface of aragonite crystals or in the intergranular space (Figure 13). Based on the form of gold (colloidal) and low Ag content (less than 5 wt %), we consider this gold secondary [1]. During hydrothermal reworking of the active system, the following changes of temperature and redox conditions promote alteration of sulphide, decomposition of tellurides and mobilize gold by the late low-temperature fluid. A fraction of the remobilized gold was “protected” and re-precipitated by abundant amorphous silica. We hypothesize that aragonite plays a role of coagulator for abundant remobilized gold from decomposed tellurides and Au-bearing primary sulphides during hydrothermal reworking of mature sulphide, as described above. The adsorption of colloidal gold by aragonite could influence the precipitation of secondary gold. This mechanism of enrichment that involves carbonate coagulant was described for on-land Au deposits by Petrovskaya [47]. As a result of this process, we supposed that the released gold is captured by the aragonite coagulant, while Te disseminates in seawater or precipitates as an isomorphic admixture in secondary sulphide minerals. Gold associated with aragonite is detected in different stations within the field. Because aragonite supports gold precipitation, the widespread distribution of aragonite formations within the hydrothermal field is a potent precondition for the gold enrichment within the mature sulphide deposits. However, in these samples, the degree of Au enrichment also depends on the Au-content in primary sulphide, which experienced reworking during the hydrothermal activity.

5.2. Factors Controlling High Content of Au and Te

The initial enrichment in Te and Au of Semyenov-2 SMS deposits is driven by deriving of Au and Te from the host rocks during hydrothermal recycling processes.

The combination of mafic, ultramafic and felsic rocks within OCC could be one of the reasons for the primary high Au and Te concentrations in Semyenov-2 SMS deposits. Elevated Au content in the host rock is recorded (Table 11). However, there are no data for Te content in the host rock within Semyenov-2. Moreover, the data of tellurium concentration in host rocks of the ocean, hydrothermal fluids and seawater are very limited. The high Te content (average 20–50 ppm but up to 200 ppm) and wide diversity of tellurium mineralization are characteristic for Ural VMS deposits, where both mafic and felsic host-rocks occur [48]. Thus, the occurrence of plagiogranites within the Semyenov hydrothermal field could have explained the initial enrichment of the hydrothermal fluid with Te.

The next important reason is favourable environments for precipitating Au and Te from the fluid. Au could precipitate as Au chloride complexes from the initial high-temperature fluid (300–400 °C) and is related to primary Cu-Fe sulphide [1,49,50]. However, the concentration of Au remains low. Likely, this could be related to the unsuitable character of the discharge of short-lived fluid. The most favourable temperature for gold precipitation is around 250–150 °C [51,52]. Low-temperature fluid transfers gold as bisulfide complexes and precipitates it with Zn-sulphide and Zn-Si assemblages [1,53]. The tellurides precipitate in a narrow temperature interval - around 260° to above 230 °C) [15]. Tellurium remains dissolved in highly reduced fluids and does not precipitate. However, tellurides are unstable in oxygen-bearing environments predominant in seawater and under temperatures below 200 °C [15,54–56]. The most favourable environments for primary Te-precipitation are from the medium-temperature portion of the fluid with a minor influence of seawater. The subsequent seawater penetration leads to decreasing temperature, increasing oxidation conditions and remobilization of Te.

An important contribution to Au-enrichment is the process of the hydrothermal re-working of the SMS deposit, in which the mechanism for the re-deposition of Au influences the increasing concentration.

6. Conclusions

The discovery and distribution of the minerals of Au and Te in various mineral assemblages delineate the favourable conditions for Au and Te enrichment in SMS from the Semyenov-2 hydrothermal field (Figure 16).

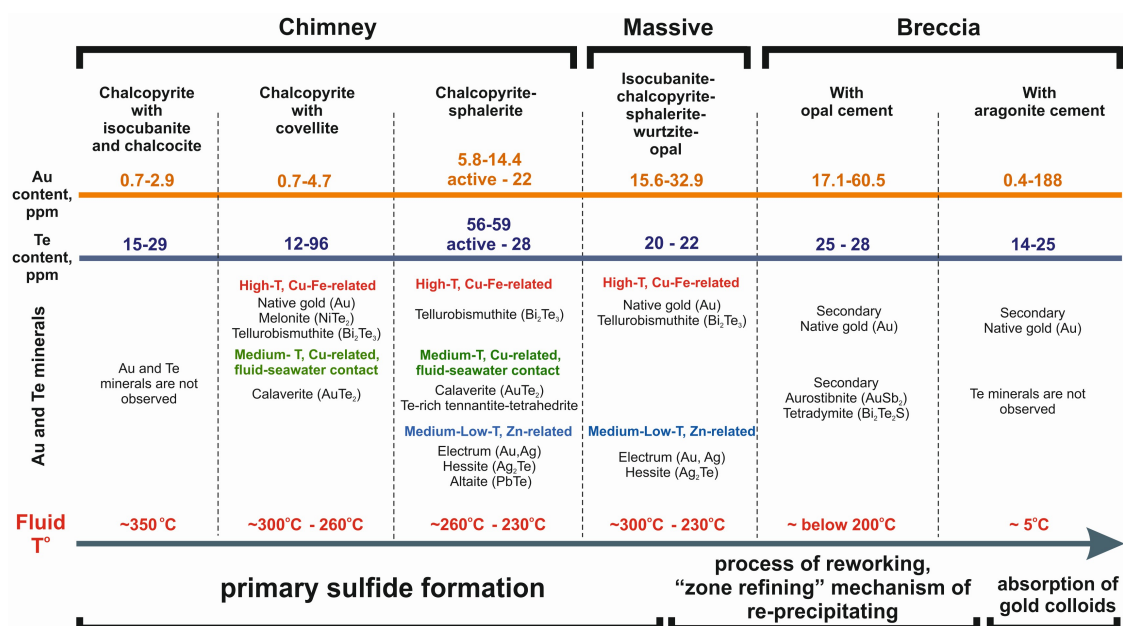


Figure 16. The distribution of Au and Te minerals in chimneys, massive sulphide and breccia from Semyenov-2 hydrothermal field.

The enrichment of Te and Au is associated with input from different source rocks and favourable environments for Au and Te precipitation (temperature of the fluid, mixing with seawater and the mechanism of deposition). Consequently, we propose that the mechanism of re-deposition of gold could be widespread for fields with long-term hydrothermal activity and where the process of re-working and "zone-refining" occurs. An additional contribution of Au-enrichment is the formation of aragonite within SMS deposits. For a better understanding of Au and Te enrichment, thermodynamic modelling is planned for SMS from Semyenov-2 in the future. A further detailed investigation of host rocks and the tectonic setting will also help us to gain a more complete understanding of the origin of high values of Au and Te.

Supplementary Materials: The following are available online at <http://www.mdpi.com/2075-163X/9/5/294/s1>, Table S1: Chemical Composition of Minerals from Semyenov-2 Hydrothermal Field (EDX data), Table S2: Chemistry of SMS Samples from Semyenov-2 Hydrothermal Field.

Author Contributions: A.F. studied samples of massive sulphide, performed the microprobe analyses, analysed the data, interpreted the results, wrote the text; T.S. collected samples and described the samples onboard, interpreted the results, wrote the text; A.S. analysed the data, wrote the text; G.C., revised the manuscript. I.P. wrote the text.

Funding: This research was partly funded by the Russian Foundation for Basic Research, project NO 18-05-00861\18.

Acknowledgments: The authors express their thanks to Larisa Lazareva, Victor Bel'tenev, Irina Rozhdstvenskaya and Victor Ivanov for the provided samples. We are grateful to Nicholas Dyriw and Sasha Turchin for reviews and editing. The authors appreciate the valuable comments and advice from the anonymous reviewers.

Conflicts of Interest: The authors declare no conflict of interest.

Abbreviations

The following abbreviations are used in this manuscript:

MAR	Mid-Atlantic Ridge
EPR	East Pacific Rise
OCC	Oceanic Core Complex
SMS	Seafloor Massive Sulfides
VMS	Volcanogenic Massive Sulphides
PDB	Pee Dee Belemnite

SMOW	Standard Mean Ocean Water
BSE	Back-Scattered Electron Detector
ICP-MS	Inductively Coupled Plasma-Mass Spectroscopy

References

- Hannington, M.D.; Thompson, G.; Rona, P.A.; Scott, S.D. Gold and native copper in supergene sulphides from the Mid-Atlantic Ridge. *Nature* **1988**, *333*, 64–66. [[CrossRef](#)]
- Hannington, M.; Herzig, P.; Scott, S.; Thompson, G.; Rona, P. Comparative mineralogy and geochemistry of goldbearing sulphide deposits on the mid-ocean ridges. *Mar. Geol.* **1991**, *101*, 217–248. [[CrossRef](#)]
- Herzig, P.M.; Hannington, M.D.; Scott, S.D.; Maliotis, G.; Rona, P.A.; Thompson, G. Gold-rich sea-floor gossans in the Troodos ophiolite and on the Mid-Atlantic Ridge. *Econ. Geol.* **1991**, *86*, 1747–1755. [[CrossRef](#)]
- Hannington, M.D.; Tivey, M.K.; Larocque, A.C.L.; Petersen, S.; Rona, P. The occurrence of gold in sulphide deposits of the TAG hydrothermal field, Mid-Atlantic Ridge. *Can. Miner.* **1995**, *33*, 1285–1310.
- Petersen, S.; Kuhn, T.; Herzig, P.M.; Hannington, M.D. Factors controlling precious and base-metal enrichments at the ultramafic-hosted Logatchev hydrothermal field, 14°45′N on the MAR; new insights from cruise M60/3. In *Mineral Deposit Research: Meeting the Global Challenge, Proceedings of the 8th Biennial SGA Meeting, Beijing, China, 18–21 August 2005*; Mao, J., Bierlein, F.P., Eds.; Springer: Berlin, Germany, 2005; pp. 679–682.
- Hannington, M.D.; de Ronde, C.E.J.; Petersen, S. *Sea-Floor Tectonics and Submarine Hydrothermal Systems*; Economic Geology 100th Anniversary Volume; Society of Economic Geologists: Littelton, CO, USA, 2005; pp. 111–141. [[CrossRef](#)]
- Rona, P.A.; Hannington, M.D.; Raman, C.V.; Thompson, G.; Tivey, M.K.; Humphris, S.E.; Lalou, C.; Petersen, S. Active and relict seafloor hydrothermal mineralization at the TAG hydrothermal field, Mid-Atlantic Ridge. *Econ. Geol.* **1993**, *88*, 1989–2017. [[CrossRef](#)]
- Lein, A.Yu.; Cherkashov, G.A.; Ul'yanov, A.A.; Ul'yanova, N.V.; Stepanova, T.V.; Sagalevich, A.M.; Bogdanov, Yu.A.; Gurvich, E.G.; Torokhov, M.P. Mineralogy and geochemistry of sulphide ores from the Logachev-2 and Rainbow fields: Similar and distinctive features. *Geochem. Int.* **2003**, *41*, 271–294.
- Fouquet, Y.; Cambon, P.; Etoubleau, J.; Charlou, J.; Ondréas, H.; Barriga, F.; Cherkashov, G.; Semkova, T.; Poroshina, I.; Bohn, M.; et al. Geodiversity of hydrothermal processes along the Mid-Atlantic Ridge and ultramafic-hosted mineralization: A new type of oceanic Cu-Zn-Co-Au volcanogenic massive sulphide deposit. In *Diversity of Hydrothermal Systems on Slow Spreading Ocean Ridges, Geophysical Monograph Series*; Rona, P., Devey, C., Dymont, J., Murton, B., Eds.; American Geophysical Union: Washington, DC, USA, 2010; Volume 188, pp. 321–368.
- Firstova, A.; Stepanova, T.; Cherkashov, G.; Goncharov, A.; Babaeva, S. Composition and Formation of Gabbro-Peridotite Hosted Seafloor Massive Sulphide Deposits from the Ashadze-1 Hydrothermal Field, Mid-Atlantic Ridge. *Minerals* **2016**, *6*, 19. [[CrossRef](#)]
- Hannington, M.D.; Peter, J.M.; Scott, S.D. Gold in seafloor polymetallic sulphide deposits. *Econ. Geol.* **1986**, *81*, 1867–1883. [[CrossRef](#)]
- Melekestseva, I.Y.; Maslennikov, V.V.; Tret'yakov, G.A.; Nimis, P.; Beltenev, V.E.; Rozhdestvenskaya, I.I.; Maslennikova, S.P.; Belogub, E.V.; Danyushevsky, L.; Large, R.; et al. Gold- and Silver-Rich Massive Sulphides from the Semenov-2 Hydrothermal Field, 13°31.13′N, Mid-Atlantic Ridge: A Case of Magmatic Contribution? *Econ. Geol.* **2017**, *112*, 741–773. [[CrossRef](#)]
- Ivanov, V.N.; Beltenev, V.E.; Stepanova, T.V.; Lazareva, L.I.; Samovarov, M.L. Sulphide ores of the new hydrothermal field at the 13°31′N of the MAR. In *Metallogeny of Ancient and Modern Ocean—2008: Ore Bearing Complexes and Ore Facies*; Zaykov, V.V., Ed.; Institute of Mineralogy: Miass, Russia, 2008; pp. 19–22. (in Russian)
- Zierenberg, R.A.; Koski, R.A.; Morton, J.L.; Bouse, R.M. Genesis of massive sulphide deposits on a sediment-covered spreading centre, Escanaba trough, southern Gorda Ridge. *Econ. Geol.* **1993**, *88*, 2069–2098. [[CrossRef](#)]
- Maslennikov, V.V.; Maslennikova, S.P.; Large, R.R.; Danyushevsky, L.V.; Herrington, R.J.; Stanley, C.J. Tellurium-bearing minerals in zoned sulphide chimneys from Cu-Zn massive sulphide deposits of the Urals, Russia. *Mineral. Petrol.* **2013**, *107*, 67–99. [[CrossRef](#)]

16. Firstova, A.; Cherkashov, G.; Stepanova, T.; Babaeva, S. Rare elements in seafloor massive sulphides of the Semyenov hydrothermal cluster, Mid-Atlantic Ridge. In Proceedings of the UMI 2014—Harvesting Seabed Mineral Resources in Harmony with Nature: 43rd Underwater Mining Institute, Lisbon, Portugal, 21–28 September 2014; pp. 131–139.
17. Smith, D.K.; Cann, J.R.; Escartín, J. Widespread active detachment faulting and core complex formation near 13°N on the Mid-Atlantic Ridge. *Nature* **2006**, *443*, 440–444. [[CrossRef](#)]
18. Smith, D.K.; Escartín, J.; Schouten, H.; Cann, J.R. Fault rotation and core complex formation: Significant processes in seafloor formation at slow-spreading mid-ocean ridges (Mid-Atlantic Ridge, 13°–15°N). *Geochem. Geophys. Geosystems* **2008**, *9*, Q03003. [[CrossRef](#)]
19. MacLeod, C.J.; Searle, R.C.; Casey, J.F.; Mallows, C.; Unsworth, M.; Achenbach, K.; Harris, M. Life cycle of oceanic core complexes. *Earth Planet. Sci. Lett.* **2009**, *287*, 333–344. [[CrossRef](#)]
20. Mallows, C.; Searle, R.C. A geophysical study of oceanic core complexes and surrounding terrain, Mid-Atlantic Ridge 13°N–14°N. *Geochem. Geophys. Geosystems* **2012**, *13*, Q0AG08. [[CrossRef](#)]
21. Escartín, J.; Mevel, C.; Petersen, S.; Bonnemains, D.; Cannat, M.; Andreani, M.; Godard, M. Tectonic structure, evolution and the nature of oceanic core complexes and their detachment fault zones (13°20'N and 13°30'N, Mid Atlantic Ridge). *Geochem. Geophys. Geosystems* **2017**, *18*, 1451–1482. [[CrossRef](#)]
22. Cann, J.R.; Blackman, D.K.; Smith, D.K.; McAllister, E.; Janssen, B.; Mello, S.; Aygerinos, E.; Pascoe, A.R.; Escartín, J. Corrugated slip surfaces formed at North Atlantic ridge-transform intersections. *Nature* **1997**, *385*, 329–332. [[CrossRef](#)]
23. Tucholke, B.E.; Lin, J.; Kleinrock, M.C. Megamullions and mullion structure defining oceanic metamorphic core complexes on the Mid-Atlantic Ridge. *J. Geophys. Res.* **1998**, *103*, 9857–9866. [[CrossRef](#)]
24. MacLeod, C.J.; Escartín, J.; Banerji, D.; Banks, G.J.; Gleeson, M.; Irving, D.H.B.; Smith, D.K. Direct geological evidence for oceanic detachment faulting: The Mid-Atlantic Ridge, 15°45'N. *Geology* **2002**, *30*, 879–882. [[CrossRef](#)]
25. Escartín, J.; Mevel, C.; MacLeod, C.J.; McCaig, A.M. Constraints on deformation conditions and the origin of oceanic detachments: The Mid-Atlantic Ridge core complex at 15°45'N. *Geochem. Geophys. Geosystems* **2003**, *4*, 1067. [[CrossRef](#)]
26. Pertsev, A.N.; Bortnikov, N.S.; Vlasov, E.A.; Beltenev, V.E.; Dobretsova, I.G.; Ageeva, O.A. Recent massive sulphide deposits of the Semenov ore district, Mid-Atlantic Ridge, 13°31' N: Associated rocks of the oceanic core complex and their hydrothermal alteration. *Geol. Ore Depos.* **2012**, *54*, 334–346. [[CrossRef](#)]
27. Beltenev, V.; Ivanov, V.; Rozhdestvenskaya, I.; Cherkashov, G.; Stepanova, T.; Shilov, V.; Davydov, M.; Laiba, A.; Kaylio, V.; Narkevsky, E.; et al. New data about hydrothermal fields on the Mid-Atlantic Ridge between 11°–14°N: 32nd cruise of R/V Professor Logatchev. *InterRidge News* **2009**, *18*, 14–18.
28. PMGE. Unpublished PMGE report on regional works on a scale of 1:500,000–1:1,000,000 for deep-sea polymetallic sulphides in the axial zone of the Mid-Atlantic Ridge and searching works at Ashadze hydrothermal field: Polar Marine Geosurvey Expedition, Lomonosov-St-Petersburg. 2007; Unpublished report. 67p. (in Russian)
29. PMGE. Unpublished PMGE report on regional works for deep-sea polymetallic sulphides in the axial zone of the Mid-Atlantic Ridge: Polar Marine Geosurvey Expedition, Lomonosov-St-Petersburg. 2009; Unpublished report. 75p. (in Russian)
30. Melekestseva, I.Y.; Kotlyarov, V.A.; Khvorov, P.V.; Ivanov, V.N.; Beltenev, V.E.; Dobretsova, I.G. Noble-metal mineralization in the Semenov-2 hydrothermal field (13°31'N), Mid-Atlantic Ridge. *Geol. Ore Depos.* **2010**, *52*, 800–810. [[CrossRef](#)]
31. Böhm, F.; Dullo, W.-Ch.; Joachimski, M.M.; Eisenhauer, A. Oxygen isotope fractionation in marine aragonite of coralline sponges. *Geochim. Cosmochim. Acta* **2000**, *64*, 1695–1703. [[CrossRef](#)]
32. Bonatti, E.; Lawrence, J.R.; Hamlyn, P.R.; Breger, D. Aragonite from deep-sea ultramafic rocks. *Geochim. Cosmochim. Acta* **1980**, *44*, 1207–1214. [[CrossRef](#)]
33. Thompson, G.; Livingston, H.D. Strontium and uranium concentrations in aragonite precipitated by some modern corals. *Earth Planet. Sci. Lett.* **1970**, *8*, 439–442. [[CrossRef](#)]
34. Dubinina, E.O.; Chernyshov, I.V.; Bortnikov, N.S.; Lein, A.Y. Isotopic and geochemical features of hydrothermal field Lost-City. *Geochemistry* **2007**, *11*, 1223–1236. (in Russian).

35. Früh-Green, G.L.; Kelley, D.S.; Bernasconi, S.M.; Karson, J.A.; Ludwig, K.A.; Butterfield, D.A.; Boschi, C.; Proskurowski, G. 30,000 years of hydrothermal activity at the Lost City vent field. *Science* **2003**, *301*, 495–498. [[CrossRef](#)]
36. Lein, A.Yu.; Galkin, S.V.; Maslennikov, V.V. New type of carbonate rocks on the ocean floor. *Rep. Acad. Sci.* **2007**, *412*, 535–539. (in Russian).
37. Mozgova, N.N.; Trubkin, N.V.; Borodaev, Y.S.; Cherkashov, G.A.; Stepanova, T.V.; Semkova, T.A.; Uspenskaya, T.Y. Mineralogy of massive sulphides from the Ashadze hydrothermal field, 13°N, Mid-Atlantic Ridge. *Can. Miner.* **2008**, *46*, 545–567. [[CrossRef](#)]
38. Taylor, S.R. Trace element abundances and the chondritic Earth model. *Geochim. Cosmochim. Acta* **1964**, *28*, 1989–1998. [[CrossRef](#)]
39. Vinogradov, A.P. The average content of chemical elements in the main types of igneous rocks of the earth's crust. *Geochemistry* **1962**, *7*, 641–664. (in Russian).
40. Turekian, K.K.; Wedepohl, K.H. Distribution of the elements in some major units of the Earth's crust. *Geol. Soc. Am. Bull.* **1961**, *72*, 175–192. [[CrossRef](#)]
41. Foster, R.P. *Gold metallogeny and Exploration*; Springer: New York, NY, USA, 1991; 432p.
42. Silantyev, S.A.; Kubrakova, I.V.; Tyutyunnik, O.A. The distribution pattern of siderophilic and chalcophilic elements in the serpentinites of the oceanic lithosphere is a reflection of the magmatic and intracrustal evolution of the mantle substrate. *Geochemistry* **2016**, *12*, 1059–1075. (in Russian).
43. Maslennikov, V.V.; Maslennikova, S.P. Rare mineral assemblages in black and white smoker vent chimneys from Uralian VHMS deposits, Russia. In *Mineral Deposit Research: Meeting the Global Challenge, Proceedings of the Eighth Biennial SGA Meeting, Beijing, China, 18–21 August 2005*; Mao, J., Bierlein, F.P., Eds.; Springer: Berlin, Germany, 2005; pp. 647–650.
44. Afifi, A.M.; Kelly, W.C.; Essene, E.J. Phase relations among tellurides, sulphides and oxides: I. Thermodynamical data and calculated equilibria. *Econ. Geol.* **1988**, *83*, 377–394. [[CrossRef](#)]
45. Jaireth, S. Hydrothermal geochemistry of Te, Ag₂Te and AuTe₂ in epithermal precious metal deposits. *EGRU Contrib.* **1991**, *37*, 1–21.
46. Fouquet, Y.; Wafik, A.; Cambon, P.; Mevel, C.; Meyer, G.; Gente, P. Tectonic setting and mineralogical and geochemical zonation in the Snake Pit sulphide deposit (Mid-Atlantic Ridge at 23° N). *Econ. Geol.* **1993**, *88*, 2018–2036. [[CrossRef](#)]
47. Petrovskaya, N.V. *Native Gold*; Science: Moscow, Russia, 1973; 350p.
48. Prokin, V.A.; Buslaev, F.P. Massive copper-zinc sulphide deposits in the Urals. *Ore Geol. Rev.* **1998**, *14*, 1–69. [[CrossRef](#)]
49. Helgeson, H.C. Thermodynamics of hydrothermal systems at elevated temperatures and pressures. *Am. J. Sci.* **1969**, *267*, 729–804. [[CrossRef](#)]
50. Henley, R.W. Solubility of gold in hydrothermal chloride solutions. *Chem. Geol.* **1973**, *11*, 73–87. [[CrossRef](#)]
51. Shernberger, D.M.; Barnes, H.L. Solubility of gold in aqueous sulphide solutions from 150 to 250 °C. *Geochim. Cosmochim. Acta* **1989**, *53*, 269–278. [[CrossRef](#)]
52. Hannington, M.D.; Scott, S.D. Sulfidation equilibria as guides to gold mineralization in volcanogenic massive sulphides; evidence from sulphide mineralogy and the composition of sphalerite. *Econ. Geol.* **1989**, *84*, 1978–1995. [[CrossRef](#)]
53. Seward, T.M. Thio complexes of gold and the transport of gold in hydrothermal ore solutions. *Geochim. Cosmochim. Acta* **1973**, *37*, 379–399. [[CrossRef](#)]
54. Oudin, E.; Constantinou, G. Black smoker chimney fragments in Cyprus sulphide deposits. *Nature* **1984**, *308*, 349–353. [[CrossRef](#)]
55. Little, C.T.S.; Maslennikov, V.V.; Morris, N.J.; Gubanov, A.P. Two Palaeozoic hydrothermal vent communities from the Southern Ural Mountains, Russia. *Palaentology* **1999**, *42*, 1043–1078. [[CrossRef](#)]
56. Eremin, N.I. *Differentiation of Volcanogenic Sulphide Mineralization*; Moscow University: Moscow, Russia, 1983; 256p.

